

Intrinsic finite-energy Cooper pairing in $j = 3/2$ superconductors

Masoud Bahari,^{1,2,*} Song-Bo Zhang,^{1,2} and Björn Trauzettel^{1,2}

¹*Institute for Theoretical Physics and Astrophysics, University of Würzburg, D-97074 Würzburg, Germany*

²*Würzburg-Dresden Cluster of Excellence ct.qmat, Germany*

(Dated: November 19, 2021)

We show that Cooper pairing can occur intrinsically away from the Fermi surface in $j = 3/2$ superconductors with strong spin-orbit coupling and equally curved bands in the normal state. In contrast to conventional pairing between spin-1/2 electrons, we derive that pairing can happen between inter-band electrons having different magnetic quantum numbers, for instance, $m_j = 1/2$ and $m_j = 3/2$. Such superconducting correlations manifest themselves by a pair of indirect gap-like structures at finite excitation energies. An observable signature of this exotic pairing is the emergence of a pair of symmetric superconducting coherence peaks in the density of states at finite energies. Moreover, the angular-momentum-resolved density of states in the presence of a perturbative Zeeman field reflects the m_j composition of the Cooper pairs. We argue that such finite-energy pairing is a generic feature of $j = 3/2$ superconductors, both in presence and absence of inversion symmetry.

Introduction.—Since the discovery of Bardeen–Cooper–Schrieffer theory for superconductivity [1], extensive efforts of theoretical and experimental research have been carried out to understand the pairing mechanism [2, 3]. In most cases, superconductivity can be described by pairing of spin-1/2 electrons at the Fermi surface. However, it has been shown theoretically that pairing of electrons with higher total angular momentum is also possible [4–6]. This has triggered attempts to formulate a general theory of high angular momentum superconductivity [7–10] and to identify typical physical observables [11–22]. Prominent candidate materials for high angular momentum superconductivity are half-Heusler compounds whose Fermi surface lies close to the Γ_8 band with total angular momentum quantum number $j = 3/2$ [23–41]. These materials can be categorized into two distinct groups with inverted [23–36, 38–42] and normal [31, 37, 38, 41] band structures, respectively. In the inverted case, only a single pair of Γ_8 bands with identical components of total angular momentum cross the Fermi energy [6, 42–45]. Despite the $j = 3/2$ nature of the electrons, the pairing mechanism in this case can be captured within the formalism for (pseudo)spin-1/2 electrons at low energies [6]. In contrast, in the group with normal band structure, density functional theory calculations predict that all Γ_8 bands bend downward near the Fermi energy [24, 25, 41, 43–45]. This band structure applies, for instance, to $RPdBi$ with $R \in \{Y, Dy, Tb, Sm\}$ [31, 37, 38, 41, 46]. We demonstrate below that such configuration of energy bands in combination with superconductivity allow us to observe Cooper pairing composed by electrons with non-identical magnetic quantum numbers m_j at finite excitation energies (FEE).

Pairing of spin-1/2 electrons with different orbitals at FEE has been proposed for the material MgB_2 in absence of spin-orbit coupling [47]. Recently, it has been argued that Ising superconductors may realize finite-energy pair-

ing of spin-1/2 electrons by applying external in-plane magnetic fields [48].

Hence, the novel question we address in this Letter is whether it is possible to observe intrinsic finite-energy Cooper pairing composed by electrons with *different* magnetic quantum numbers in the absence of any fields. We show below that the interplay of strong spin-orbit coupling and superconductivity allows for such pairing accompanied by a pair of indirect *gap-like structures* (GLSs) away from the Fermi energy. The electrons responsible for the finite-energy pairing originate from energy bands with different band indices. Our results suggest that such behavior is a generic feature of multiband superconductors when the $j = 3/2$ electrons of the Γ_8 band contribute to pairing. In experiments, the GLSs manifest themselves by the appearance of a pair of symmetric superconducting coherence peaks at FEE of the density of states (DOS). To elucidate that such novel Cooper pairing is a generic phenomenon of multi-band superconductors preserving (breaking) inversion symmetry, we systematically analyze the role of $j = 3/2$ pairing valid for cubic point group symmetry O_h (T_d) based on the Luttinger–Kohn model.

Model.—Low-energy $j = 3/2$ electrons within the Γ_8 bands can be described by the $\mathbf{k}\cdot\mathbf{p}$ Luttinger-Kohn model [49, 50], $H_0 = \sum_{\mathbf{k}} \hat{c}_{\mathbf{k}}^\dagger \hat{\mathcal{H}}_0(\mathbf{k}) \hat{c}_{\mathbf{k}}$, where

$$\hat{\mathcal{H}}_0(\mathbf{k}) = \alpha k^2 \hat{I}_4 + \beta \sum_i k_i^2 \hat{J}_i^2 + \gamma \sum_{i \neq j} k_i k_j \hat{J}_i \hat{J}_j - \mu \hat{I}_4, \quad (1)$$

and the basis is $\hat{c}_{\mathbf{k}} = (c_{\mathbf{k},3/2}, c_{\mathbf{k},1/2}, c_{\mathbf{k},-1/2}, c_{\mathbf{k},-3/2})^T$. We denote $\mathbf{k} = (k_x, k_y, k_z)$ as the 3D momentum, $k = |\mathbf{k}|$, \hat{J}_i with $i \in \{x, y, z\}$ as the 4×4 total angular momentum matrices in $j = 3/2$ representation, and \hat{I}_4 as the 4×4 identity matrix. The material-dependent parameters α and β (γ) control kinetic energy and symmetric spin-orbit coupling, respectively; μ is the Fermi energy. The doubly-degenerate eigenenergies of $\hat{\mathcal{H}}_0(\mathbf{k})$, protected

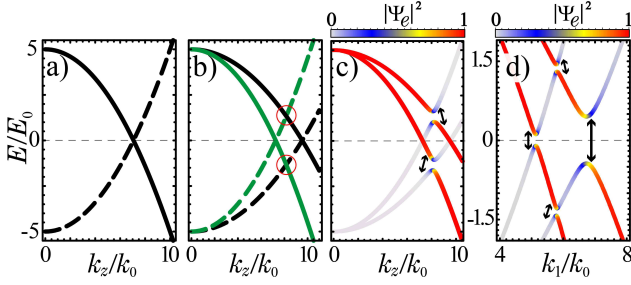


Fig. 1. BdG spectra along the $[0, 0, 1]$ direction in absence of pairing for (a) $\beta = 0$ and (b) $\beta = 0.2|\alpha|$, respectively. The spectra are independent of γ . BdG spectrum in the (c) $[0, 0, 1]$ and (d) $[1, 1, 0]$ (i.e., $k_x = k_y = k_1$) directions for $\gamma = \beta$ in presence of septet pairing with amplitude $\Delta/E_0 a = 4.15$. The color denotes the probability of electronic states $|\Psi_e|^2$ in both (c) and (d) panels. Other parameters are $\mu/E_0 = -5$, $k_0 = 10^{-2}a^{-1}$, $E_0 = 10^{-3}|\alpha|a^{-2}$ and $\alpha = -20$. a is the lattice constant in a tight-binding version of the continuum model.

by the combination of inversion and time-reversal symmetries, are given by

$$E_{\mathbf{k}}^{\pm} = \left(\alpha + \frac{5}{4}\beta \right) k^2 \pm \beta \sqrt{\sum_i \left[k_i^4 + \left(\frac{3\gamma^2}{\beta^2} - 1 \right) k_i^2 k_{i+1}^2 \right]} - \mu, \quad (2)$$

where $i+1 = y$ if $i = x$ (notation used throughout the paper). To investigate the properties of the excitation spectrum of Eq. (1) in the presence of high angular momentum Cooper pairing in O_h symmetry, we introduce the full superconducting Hamiltonian given by $H = \sum_{\mathbf{k}} \hat{\psi}_{\mathbf{k}}^{\dagger} \hat{H}_{\text{BdG}}(\mathbf{k}) \hat{\psi}_{\mathbf{k}}$, where $\hat{\psi}_{\mathbf{k}} = (\hat{c}_{\mathbf{k}}, \hat{c}_{-\mathbf{k}}^{\dagger T})^T$ is the Nambu spinor. The Bogoliubov-de Gennes (BdG) Hamiltonian takes the form

$$\hat{H}_{\text{BdG}}(\mathbf{k}) = \begin{pmatrix} \hat{H}_0(\mathbf{k}) & \hat{H}_{\eta}^{J,S,L}(\mathbf{k}) \\ [\hat{H}_{\eta}^{J,S,L}(\mathbf{k})]^{\dagger} & -\hat{H}_0^T(-\mathbf{k}) \end{pmatrix}, \quad (3)$$

where $\hat{H}_{\eta}^{J,S,L}(\mathbf{k})$ is the pairing Hamiltonian in channel (η, J, S, L) with η being the relative basis label of the cubic irreducible representation (IR) [51, 52]. The channel of instability is named by Cooper pair quantum numbers with total angular momentum J combining intrinsic spin S and orbital L angular momenta [8, 9, 53].

To shed light on finite-energy pairing, the BdG excitation spectrum along the $[0, 0, 1]$ direction in absence of spin-orbit coupling and pairing is plotted in Fig. 1(a). The fourfold degenerate electron bands (solid line) cross their hole counterparts (dashed line) at $k_F = \sqrt{\mu/\alpha}$. A finite β accounting for spin-orbit coupling splits the energy bands having different magnetic quantum numbers. Increasing β , this moves the crossings at the Fermi surface $E = 0$ and at FEE (red circles), as shown in Fig. 1(b). The low-energy m_j split Fermi momenta consist of $m_j = 1/2$ states (green) and $m_j = 3/2$ states (black) located at $k_F^- = 2\sqrt{\mu/(4\alpha + \beta)}$ and $k_F^+ = 2\sqrt{\mu/(4\alpha + 9\beta)}$, respectively. Moreover, the finite-energy crossing appears at $k = 2\sqrt{\mu/(4\alpha + 5\beta)}$ incorporating $m_j = 3/2$

electron (hole) and $m_j = 1/2$ hole (electron) states at positive (negative) excitation energies. In the superconducting state, the pairing mechanism occurs not only at $E = 0$ but also at FEE [Figs. 1(c) and 1(d)]. Notably, the finite-energy pairing can be present when the low-energy intra-band states exhibit nodal [Fig. 1(c)] or gapped excitation spectra [Fig. 1(d)].

Finite-energy effective theory.—To better understand the finite-energy pairing, we develop an effective theory close to the FEE. We start by obtaining the band basis representation of the BdG Hamiltonian through the basis transformation $\hat{c}_{\mathbf{k}} = \hat{V}_{\mathbf{k}}^+ \hat{f}_{\mathbf{k}}^+ + \hat{V}_{\mathbf{k}}^- \hat{f}_{\mathbf{k}}^-$, where $\hat{V}_{\mathbf{k}}^{\pm}$ is a 4×2 matrix containing the eigenvectors corresponding to $E_{\mathbf{k}}^{\pm}$. Note that $\hat{f}_{\mathbf{k}}^{\pm} = (f_{\mathbf{k},\uparrow}^{\pm}, f_{\mathbf{k},\downarrow}^{\pm})^T$ and $f_{\mathbf{k},s}^{\pm}$ ($f_{\mathbf{k},s}^{\pm\dagger}$) annihilates (creates) a state with pseudospin degrees of freedom $s \in \{\uparrow, \downarrow\}$ in the band basis labeled by \pm in Eq. (2). To capture the inter-band superconducting Hamiltonian, we choose our basis set as $\hat{\phi}_{\mathbf{k}} = (\hat{\phi}_{\mathbf{k}}^{+-}, \hat{\phi}_{\mathbf{k}}^{-+})^T$ with $\hat{\phi}_{\mathbf{k}}^{+-} = (\hat{f}_{\mathbf{k}}^+, (\hat{f}_{-\mathbf{k}}^-)^T)^T$ denoting the electron-hole subspace basis with band index $(+, -)$ and $\hat{\phi}_{\mathbf{k}}^{-+} = (\hat{f}_{\mathbf{k}}^-, (\hat{f}_{-\mathbf{k}}^+)^T)^T$. Thus, we rewrite the superconducting Hamiltonian in the band basis as $H = \sum_{\mathbf{k}} \hat{\phi}_{\mathbf{k}}^{\dagger} \hat{h}(\mathbf{k}) \hat{\phi}_{\mathbf{k}}$ with

$$\hat{h}(\mathbf{k}) = \begin{pmatrix} E_{\mathbf{k}}^+ & \hat{\Delta}_{\mathbf{k}}^{+-} & 0 & \hat{\Delta}_{\mathbf{k}}^{++} \\ (\hat{\Delta}_{\mathbf{k}}^{+-})^{\dagger} & -E_{\mathbf{k}}^- & (\hat{\Delta}_{\mathbf{k}}^{--})^{\dagger} & 0 \\ 0 & \hat{\Delta}_{\mathbf{k}}^{--} & E_{\mathbf{k}}^- & \hat{\Delta}_{\mathbf{k}}^{-+} \\ (\hat{\Delta}_{\mathbf{k}}^{++})^{\dagger} & 0 & (\hat{\Delta}_{\mathbf{k}}^{-+})^{\dagger} & -E_{\mathbf{k}}^+ \end{pmatrix}, \quad (4)$$

where $\hat{\Delta}_{\mathbf{k}}^{+-}$ is the projection of the pairing instability onto the inter-band basis given by $\hat{\Delta}_{\mathbf{k}}^{+-} = \hat{V}_{\mathbf{k}}^{+\dagger} \hat{\mathcal{H}}_{\eta}^{J,S,L}(\mathbf{k}) (\hat{V}_{-\mathbf{k}}^-)^T$. Treating the off-diagonal blocks, corresponding to the intra-band pairing denoted by $\hat{\Delta}_{\mathbf{k}}^{\nu\nu}$ with $\nu \in \{+, -\}$, as a perturbation to the inter-band diagonal block and employing the folding down approach [54], we arrive at the effective Hamiltonian valid in the vicinity of the GLSs

$$H_{\text{eff}}^{+-}(\mathbf{k}) = \begin{pmatrix} E_{\mathbf{k}}^+ + \hat{\varepsilon}_{\mathbf{k}}^{++} & \hat{\Delta}_{\text{eff}}^{+-}(\mathbf{k}) \\ (\hat{\Delta}_{\text{eff}}^{+-}(\mathbf{k}))^{\dagger} & -E_{\mathbf{k}}^- + \hat{\varepsilon}_{\mathbf{k}}^{--} \end{pmatrix}. \quad (5)$$

The second term on the diagonal in Eq. (5) is a pseudospin energy shift induced by the pairing of intra-band quasi-particles, given by $\hat{\varepsilon}_{\mathbf{k}}^{\nu\nu} = \hat{\Delta}_{\mathbf{k}}^{\nu\nu} (\hat{\Delta}_{\mathbf{k}}^{\nu\nu})^{\dagger} / (\omega + \nu E_{\mathbf{k}}^{\nu})$. Notably, Eq. (5) is different from a typical BdG Hamiltonian. The effective particle-hole symmetry is broken due to the presence of non-identical diagonal entries arising from the nature of two different energy bands. The inter-band pairing of the effective Hamiltonian takes the form

$$\hat{\Delta}_{\text{eff}}^{+-}(\mathbf{k}) = \hat{\Delta}_{\mathbf{k}}^{+-} + \varepsilon_{\mathbf{k}}^{-1} \hat{\Delta}_{\mathbf{k}}^{++} (\hat{\Delta}_{\mathbf{k}}^{-+})^{\dagger} \hat{\Delta}_{\mathbf{k}}^{--}, \quad (6)$$

where $\varepsilon_{\mathbf{k}} = (\omega + E_{\mathbf{k}}^+) (\omega - E_{\mathbf{k}}^-)$ [55]. In the weak-pairing limit, the second term is small close to the GLSs and can be neglected. The spectrum for the FEE reads

$$\mathcal{E}_{\pm}(\mathbf{k}) = \varepsilon_{\mathbf{k},1} + \varepsilon_{\mathbf{k},2} \pm \sqrt{(\varepsilon_{\mathbf{k},1} - \varepsilon_{\mathbf{k},2})^2 + \hat{\delta}(\mathbf{k})}, \quad (7)$$

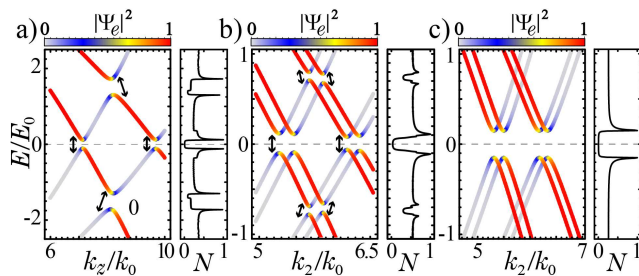


Fig. 2. BdG spectra in (a) $[0, 0, 1]$ and (b and c) $[1, 0, 1]$ (with $k_x = k_z = k_2$) directions for (a) $(\Delta/E_0a, \delta/E_0a) = (3.5, 10)$, (b) $(1.5, 2.5)$, and (c) $(0.15, 2.5)$, respectively. (a) and (b) correspond to septet pairing, and (c) corresponds to A_{1g} pairing. The corresponding density of states N normalized with respect to its maximum value are presented in the right panel of each spectrum. $\gamma = -0.05|\alpha|$ and other parameters are the same as those in Fig. 1.

where

$$\delta(\mathbf{k}) = \frac{1}{2} \text{Tr}(\hat{\Delta}_{\text{eff}}^{+-}(\mathbf{k})[\hat{\Delta}_{\text{eff}}^{+-}(\mathbf{k})]^\dagger), \quad (8)$$

is the magnitude of the GLS indicating superconducting hybridization between inter-band states [56], i.e., pairing of $m_j = 3/2$ with $m_j = 1/2$ states; Tr stands for the trace of the matrix; $\varepsilon_{\mathbf{k},1} = (1/2)E_{\mathbf{k}}^+ + (1/4)\text{Tr}(\hat{\varepsilon}_{\mathbf{k}}^{++})$ and $\varepsilon_{\mathbf{k},2} = -(1/2)E_{\mathbf{k}}^- + (1/4)\text{Tr}(\hat{\varepsilon}_{\mathbf{k}}^{--})$. The width of the GLSs around the finite-energy crossing momentum [57] is $|\mathcal{E}_+(\tilde{\mathbf{k}}) - \mathcal{E}_-(\tilde{\mathbf{k}})| = 2[\delta(\tilde{\mathbf{k}})]^{1/2}$. Note that the matrix form of $\hat{\Delta}_{\text{eff}}^{+-}(\mathbf{k})$ depends on the choice of basis while $\delta(\mathbf{k})$ is a basis-independent observable.

Symmetry properties.—Interestingly, the symmetry properties of the finite-energy pairing are different from their low-energy counterpart. For instance, we may witness even(odd)-parity pseudo-spin triplet (singlet) pairing at FEE. This is a direct consequence of the Pauli exclusion principle taking into account the exchange of band-indices in addition to the exchange of magnetic quantum numbers, i.e.,

$$\hat{\Delta}_{\text{eff}}^{+-}(-\mathbf{k}) = -[\hat{\Delta}_{\text{eff}}^{-+}(\mathbf{k})]^T. \quad (9)$$

In this sense, we can span $\hat{\Delta}_{\text{eff}}^{+-}(\mathbf{k})$ in the inter-band basis as $\hat{\Delta}_{\text{eff}}^{+-}(\mathbf{k}) = \mathbf{g}^{+-}(\mathbf{k}) \cdot \boldsymbol{\tau}$, where the four-component vector $\mathbf{g}^{+-} = (\mathbf{g}_0^{+-}, \mathbf{g}_x^{+-}, \mathbf{g}_y^{+-}, \mathbf{g}_z^{+-})$ is a complex momentum dependent function, $\boldsymbol{\tau} = (\tau_0, \tau_x, \tau_y, \tau_z)$ with $\tau_{x,y,z}$ being the Pauli matrices and τ_0 the 2×2 identity matrix in the inter-band basis. Thus, we obtain the symmetry relations

$$\mathbf{g}_{0,x,z}^{+-}(-\mathbf{k}) = -\mathbf{g}_{0,x,z}^{-+}(\mathbf{k}), \quad \mathbf{g}_y^{+-}(-\mathbf{k}) = \mathbf{g}_y^{-+}(\mathbf{k}). \quad (10)$$

This enables us to directly derive components of the $\hat{\Delta}_{\text{eff}}^{-+}(\mathbf{k})$. The y -component is even in momentum while the other components are odd [58].

Pairing channels of O_h symmetry.—We apply our theory to all time-reversal symmetric stationary pair-

$O_h (T_d)$	η	(J, S, L)	without ASOC	with ASOC
$A_{1g} (A_1)$	I	$(0, 0, 0)$	\times	\times
$A_{1u} (A_2)$	$f(\mathbf{r})$	$(0, 1, 1)$	\times	$[1, 1, 1]^*$
$T_{1u} (T_2)$	z	$(1, 1, 1)$	$[0, 0, 1]$	$[0, 0, 1]$
$E_g (E)$	$3z^2 - r^2$	$(2, 2, 0)$	$[0, 0, 1]$	\checkmark
	$x^2 - y^2$	$(2, 2, 0)$	\checkmark	\checkmark
	$3z^2 - r^2$	$(2, 3, 1)$	$[0, 0, 1]$	\checkmark
$E_u (E)$	$3z^2 - r^2$	$(2, 1, 1)$	$[0, 0, 1]^*, k_z = 0$	\checkmark
	$3z^2 - r^2$	$(2, 3, 1)$	$[0, 0, 1]$	\checkmark
	$x^2 - y^2$	$(2, 1, 1)$	$[0, 0, 1]^*$	$[0, 0, 1]$
	$x^2 - y^2$	$(2, 3, 1)$	\checkmark	\checkmark
$A_{2u} (A_1)$	xyz	$(3, 3, 1)$	$[1, 1, 1]^*$	$[1, 1, 1]^*$

Table I. Absence/presence of finite-energy Cooper pairing. The first column shows the IR of $O_h (T_d)$ point groups with η denoting the basis label of the IR. The third column corresponds to the pairing multiplets of the relative IR. The last two columns indicate presence \checkmark (absence \times) of finite-energy Cooper pairing in the entire momentum space in absence and presence of ASOC. The superscript $(*)$ means that $\delta(\mathbf{k})$ vanishes in all equivalent directions [62].

ing states of cubic point group symmetry up to the p -wave channel [9, 59] with the aim to identify inter-band pairing. To obtain analytic relations for $\delta(\mathbf{k})$, we set $\gamma = \beta$ [60]. Note that the pairing states generate cubic anisotropy. The results are summarized in Table I. Remarkably, inter-band pairing is present for a variety of pairing channels.

First, we observe that the even- and odd-parity singlet pairing states [61], corresponding to the instability channels A_{1g} and A_{1u} , respectively, have vanishing inter-band pairing, i.e., $\delta(\mathbf{k}) = 0$ [63]. Contrarily, the cubic triplet state T_{1u} [9, 64] shows finite inter-band pairing $\delta(\mathbf{k}) = \Delta^2(k_x^2 + k_y^2)$ with Δ being the pairing strength. This indicates that the GLSs are present within the whole momentum space except for the $[0, 0, 1]$ direction where inter-band pairing vanishes. Next, we focus on pairing with quintet total angular momentum, i.e., $J = 2$. In this case, the pairing state is split by the cubic field into $E_{g,u} + T_{2g,u}$ where $E_{g,u}$ ($T_{2g,u}$) is a two(three)-dimensional IR. Note that the pairing state $E_{g,u}$ is a stationary state of the free energy whereas $T_{2g,u}$ is not [9]. Hence, we focus on $E_{g,u}$ pairing in the following. The components of $E_{g,u}$ are denoted by $\eta = (3z^2 - r^2, x^2 - y^2)$. In the $j = 3/2$ representation, we find two (four) symmetry allowed pairing channels for even-parity (odd-parity) quintet pairing. For even-parity states, the quantum number is $(2, 2, 0)$, where the pairing Hamiltonian is momentum independent due to the s -wave nature of the channel. In this case, the GLSs of the $3z^2 - r^2$ state are given by $\delta(\mathbf{k}) = 3\Delta_{\mathbf{k}}^2(k_x^2 + k_y^2)(k^2 + 3k_z^2)$ with $\Delta_{\mathbf{k}} = \Delta/2k$, showing non-vanishing GLSs except for the two-fold rotation axis $[0, 0, 1]$. Importantly, the $x^2 - y^2$ state exhibits full GLSs within the entire momentum space.

The odd-parity quintet channel has four momentum

dependent stationary pairing states due to $L = 1$. The first two states correspond to the $3z^2 - r^2$ basis having Cooper pair quantum numbers $(2, 1, 1)$ and $(2, 3, 1)$. These states differ only in the intrinsic spin quantum number where $S = 1$ and $S = 3$ denote spin dipole and octupole moments, respectively. The GLS for the former state takes the form $\delta(\mathbf{k}) = 27\Delta_{\mathbf{k}}^2 (k_x^2 + k_y^2)k_z^2$. It vanishes in the $[0, 0, 1]^*$ direction [62] as well as the $k_z = 0$ plane. For the $S = 3$ channel, the GLS becomes

$$\delta(\mathbf{k}) = \Delta_{\mathbf{k}}^2 \sum_i \left[\zeta_i^{(1)} k_i^4 + \zeta_i^{(2)} k_i^2 k_{i+1}^2 \right], \quad (11)$$

with $\zeta^{(1)} = (25, 25, 0)$ and $\zeta^{(2)} = (50, 64, 64)$. In this case, $\delta(\mathbf{k})$ is present in the entire momentum space except for the z -axis.

The GLS for the p -wave $x^2 - y^2$ state in both $S = 1$ ($S = 3$) channels can also be described by Eq. (11) with coefficients $\zeta^{(1)} = (1, 1, 1)$ and $\zeta^{(2)} = (3, 0, 0)$ ($\zeta^{(1)} = (25/4, 25/4, 25)$, $\zeta^{(2)} = (103/2, 41, 41)$). Hence, the $S = 3$ channel demonstrates fully GLSs while the $S = 1$ channel exhibits vanishing $\delta(\mathbf{k})$ along the $[0, 0, 1]^*$ direction.

Finally, we look at the septet state denoted by A_{2u} . In this case, the pairing of electrons with different quantum numbers m_j manifests itself by

$$\delta(\mathbf{k}) = \frac{3\Delta_{\mathbf{k}}^2}{16} \left\{ \sum_i [4k_i^6 - 3(k_i^4 k_{i+1}^2 + k_i^4 k_{i+2}^2)] + 6k_x^2 k_y^2 k_z^2 \right\}, \quad (12)$$

where $i+2 = z$ if $i = x$ and the GLSs are present throughout the momentum space except for the $[1, 1, 1]^*$ direction.

Candidate systems with T_d structure.—It is worthwhile to note that the half-Heusler compounds $RPdBi$ have tetrahedral T_d symmetry (subgroup of O_h) without inversion center. Nevertheless, the formalism of describing the pairing is the same as for the O_h group but different IR labels apply, *cf.* Table I. The non-centrosymmetry manifests itself by an antisymmetric spin-orbit coupling (ASOC) given by [6, 65]

$$\hat{H}'(\mathbf{k}) = \delta \sum_i k_i \left(\hat{J}_{i+1} \hat{J}_i \hat{J}_{i+1} - \hat{J}_{i+2} \hat{J}_i \hat{J}_{i+2} \right), \quad (13)$$

where δ controls the strength of the ASOC and $i \in \{x, y, z\}$. Projecting $\hat{H}'(\mathbf{k})$ onto the intra-band basis, this results in splitting the energy band as $E_{\mathbf{k}}^\nu \rightarrow E_{\mathbf{k}}^\nu \pm |\mathbf{g}_{\mathbf{k}}^{\nu\nu}|$ with $\mathbf{g}_{\mathbf{k}}^{\nu\nu} \cdot \boldsymbol{\sigma} = \hat{V}_{\mathbf{k}}^{\nu\dagger} \hat{H}'(\mathbf{k}) \hat{V}_{\mathbf{k}}^\nu$ and $\nu = \pm$, as shown in Figs. 2(b) and 2(c) [66]. Here, $\mathbf{g}_{\mathbf{k}}^{\nu\nu} = (g_x^{\nu\nu}, g_y^{\nu\nu}, g_z^{\nu\nu})$ and $\boldsymbol{\sigma} = (\hat{\sigma}_x, \hat{\sigma}_y, \hat{\sigma}_z)$ are momentum dependent ASOC vector and Pauli matrices in the intra-band basis, respectively. The lack of inversion symmetry allows the pairing state to be a mixture of even-parity singlet $\hat{\mathcal{H}}_I^{0,0,0}(\mathbf{k})$ and odd-parity p -wave states [67]. In this case, the most stable odd-parity pairing state with the largest transition temperature may arise when its \mathbf{d} -vector aligns parallel to the ASOC vector [42, 68]. Thus, by combining $\hat{H}'(\mathbf{k})$ with

the Cooper pair symmetrization matrix $\hat{\mathcal{R}} = i\hat{\sigma}_x \otimes \hat{\sigma}_y$ in the $j = 3/2$ representation, we arrive at the septet pairing state $\hat{\mathcal{H}}_{xyz}^{3,3,1}(\mathbf{k}) = \hat{H}'(\mathbf{k})\hat{\mathcal{R}}$ [6]. The inter-band crossing of the mixed superconducting state $\hat{\mathcal{H}}_I^{0,0,0}(\mathbf{k}) + \hat{\mathcal{H}}_{xyz}^{3,3,1}(\mathbf{k})$ cannot be hybridized by the inversion symmetry breaking ASOC. Therefore, the emergence of finite-energy superconducting coherence peaks in the DOS are strong indicators of septet Cooper pairing of electrons with different quantum numbers m_j , as shown in Figs. 2(a) and 2(b). Note the difference to singlet pairing, where the DOS exhibit a flat shape away from the Fermi surface, *cf.* Fig. 2(c). Remarkably, both odd- and even-parity channels of $3z^2 - r^2$ turn into fully GLSs in the presence of ASOC, *cf.* Table I. This also partially happens for the A_2 state and the $(x^2 - y^2, 2, 1, 1)$ state. Therefore, a small value of ASOC even enhances the likelihood of observing GLSs in the DOS.

To observe the m_j content of the novel pairing at FEE, we propose to apply a perturbative Zeeman field to the system where the states acquire finite magnetization in terms of m_j degrees of freedom due to broken time-reversal symmetry [53]. Consequently, the GLSs split into two different pairs of GLSs. Each GLS corresponds to paired electrons with different magnetic quantum numbers signaled by simultaneous drops in the m_j -resolved DOS.

Conclusions.—We have investigated Cooper pairing in $j = 3/2$ superconductors with cubic point-group symmetry. The multiband nature of the system with identical bending configuration allows for observing Cooper pairing away from the Fermi surface in the weak pairing limit. This manifests itself by a pair of indirect finite-energy anti-crossings of BdG bands signaling pairing of electrons having different components of total angular momentum. The phenomenon may be experimentally detectable through tunneling spectroscopy [69–72] and angle-resolved photo-emission spectroscopy [73].

Note added.—During the preparation of this manuscript, we became aware of a related proposal of inter-band pairing away from the Fermi surface. This proposal is about the emergence of anapole superconductivity in the presence of competing pairing channels. Hence, the physics is different from ours [74].

We thank M. Bode, S. J. Choi, P. Eck, M. V. Hosseini, C. A. Li, G. Sangiovanni and A. H. Talebi for fruitful discussions. The work was supported by the DFG (SPP1666 and SFB1170 ToCoTronics), the Würzburg-Dresden Cluster of Excellence ct.qmat, EXC2147, Project Id 390858490, and the Elitenetzwerk Bayern Graduate School on Topological Insulators.

* masoud.bahari@physik.uni-wuerzburg.de

[1] J. Bardeen, L. N. Cooper, and J. R. Schrieffer,

- Phys. Rev. **108**, 1175 (1957).
- [2] J. P. Carbotte, *Rev. Mod. Phys.* **62**, 1027 (1990).
- [3] M. Sigrist and K. Ueda, *Rev. Mod. Phys.* **63**, 239 (1991).
- [4] T.-L. Ho and S. Yip, *Phys. Rev. Lett.* **82**, 247 (1999).
- [5] W. Yang, Y. Li, and C. Wu, *Phys. Rev. Lett.* **117**, 075301 (2016).
- [6] P. M. R. Brydon, L. Wang, M. Weinert, and D. F. Agterberg, *Phys. Rev. Lett.* **116**, 177001 (2016).
- [7] V. Kozii, J. W. F. Venderbos, and L. Fu, *Science Advances* **2**, 10.1126/sciadv.1601835 (2016).
- [8] L. Savary, J. Ruhman, J. W. F. Venderbos, L. Fu, and P. A. Lee, *Phys. Rev. B* **96**, 214514 (2017).
- [9] J. W. F. Venderbos, L. Savary, J. Ruhman, P. A. Lee, and L. Fu, *Phys. Rev. X* **8**, 011029 (2018).
- [10] P. Dutta, F. Parhizgar, and A. M. Black-Schaffer, *Phys. Rev. Research* **3**, 033255 (2021).
- [11] C. Fang, B. A. Bernevig, and M. J. Gilbert, *Phys. Rev. B* **91**, 165421 (2015).
- [12] I. Boettcher and I. F. Herbut, *Phys. Rev. B* **93**, 205138 (2016).
- [13] D. F. Agterberg, P. M. R. Brydon, and C. Timm, *Phys. Rev. Lett.* **118**, 127001 (2017).
- [14] C. Timm, A. P. Schnyder, D. F. Agterberg, and P. M. R. Brydon, *Phys. Rev. B* **96**, 094526 (2017).
- [15] J. Yu and C.-X. Liu, *Phys. Rev. B* **98**, 104514 (2018).
- [16] T. Kawakami, T. Okamura, S. Kobayashi, and M. Sato, *Phys. Rev. X* **8**, 041026 (2018).
- [17] S. Kobayashi, A. Yamakage, Y. Tanaka, and M. Sato, *Phys. Rev. Lett.* **123**, 097002 (2019).
- [18] B. Roy, S. A. A. Ghorashi, M. S. Foster, and A. H. Nvidomskyy, *Phys. Rev. B* **99**, 054505 (2019).
- [19] H. Menke, C. Timm, and P. M. R. Brydon, *Phys. Rev. B* **100**, 224505 (2019).
- [20] S.-T. Tamura, S. Imura, and S. Hoshino, *Phys. Rev. B* **102**, 024505 (2020).
- [21] C. Timm, P. M. R. Brydon, and D. F. Agterberg, *Phys. Rev. B* **103**, 024521 (2021).
- [22] A. L. Szabó, R. Moessner, and B. Roy, *Phys. Rev. B* **103**, 165139 (2021).
- [23] G. Goll, M. Marz, A. Hamann, T. Tomanic, K. Grube, T. Yoshino, and T. Takabatake, *Physica B: Condensed Matter* **403**, 1065 (2008).
- [24] H. Lin, L. A. Wray, Y. Xia, S. Xu, S. Jia, R. J. Cava, A. Bansil, and M. Z. Hasan, *Nature Materials* **9**, 546 (2010).
- [25] S. Chadov, X. Qi, J. Kübler, G. H. Fecher, C. Felser, and S. C. Zhang, *Nature Materials* **9**, 541 (2010).
- [26] N. P. Butch, P. Syers, K. Kirshenbaum, A. P. Hope, and J. Paglione, *Phys. Rev. B* **84**, 220504 (2011).
- [27] T. V. Bay, T. Naka, Y. K. Huang, and A. de Visser, *Phys. Rev. B* **86**, 064515 (2012).
- [28] F. F. Tafti, T. Fujii, A. Juneau-Fecteau, S. René de Cotret, N. Doiron-Leyraud, A. Asamitsu, and L. Taillefer, *Phys. Rev. B* **87**, 184504 (2013).
- [29] Y. Pan, A. M. Nikitin, T. V. Bay, Y. K. Huang, C. Paulsen, B. H. Yan, and A. de Visser, *EPL (Europhysics Letters)* **104**, 27001 (2013).
- [30] G. Xu, W. Wang, X. Zhang, Y. Du, E. Liu, S. Wang, G. Wu, Z. Liu, and X. X. Zhang, *Scientific Reports* **4**, 5709 (2014).
- [31] Y. Nakajima, R. Hu, K. Kirshenbaum, A. Hughes, P. Syers, X. Wang, K. Wang, R. Wang, S. R. Saha, D. Pratt, J. W. Lynn, and J. Paglione, *Science Advances* **1**, 10.1126/sciadv.1500242 (2015).
- [32] A. M. Nikitin, Y. Pan, X. Mao, R. Jeehee, G. K. Araizi, Y. K. Huang, C. Paulsen, S. C. Wu, B. H. Yan, and A. de Visser, *J. Condens. Matter Phys.* **27**, 275701 (2015).
- [33] Z. K. Liu, L. X. Yang, S.-C. Wu, C. Shekhar, J. Jiang, H. F. Yang, Y. Zhang, S.-K. Mo, Z. Hussain, B. Yan, C. Felser, and Y. L. Chen, *Nature Communications* **7**, 12924 (2016).
- [34] M. Meinert, *Phys. Rev. Lett.* **116**, 137001 (2016).
- [35] D. Shrivastava and S. P. Sanyal, *Physica C Supercond.* **544**, 22 (2018).
- [36] H. Kim, K. Wang, Y. Nakajima, R. Hu, S. Ziemak, P. Syers, L. Wang, H. Hodovanets, J. D. Denlinger, P. M. R. Brydon, D. F. Agterberg, M. A. Tanatar, R. Prozorov, and J. Paglione, *Science Advances* **4**, 10.1126/sciadv.aao4513 (2018).
- [37] H. Xiao, T. Hu, W. Liu, Y. L. Zhu, P. G. Li, G. Mu, J. Su, K. Li, and Z. Q. Mao, *Phys. Rev. B* **97**, 224511 (2018).
- [38] S. M. A. Radmanesh, C. Martin, Y. Zhu, X. Yin, H. Xiao, Z. Q. Mao, and L. Spinu, *Phys. Rev. B* **98**, 241111 (2018).
- [39] R. Majumder and M. M. Hossain, *Computational Condensed Matter* **21**, e00402 (2019).
- [40] M. M. Hosen, G. Dhakal, K. Dimitri, H. Choi, F. Kabir, C. Sims, O. Pavlosiuk, P. Wiśniewski, T. Durakiewicz, J.-X. Zhu, D. Kaczorowski, and M. Neupane, *Scientific Reports* **10**, 12343 (2020).
- [41] V. Bhardwaj, A. Bhattacharya, S. Srivastava, V. V. Khovaylo, J. Sannigrahi, N. Banerjee, B. K. Mani, and R. Chatterjee, *Scientific Reports* **11**, 7535 (2021).
- [42] K. Ishihara, T. Takenaka, Y. Miao, Y. Mizukami, K. Hashimoto, M. Yamashita, M. Konczykowski, R. Masuki, M. Hirayama, T. Nomoto, R. Arita, O. Pavlosiuk, P. Wisniewski, D. Kaczorowski, and T. Shibauchi, (2021), [arXiv:2110.01819](https://arxiv.org/abs/2110.01819).
- [43] W. Al-Sawai, H. Lin, R. S. Markiewicz, L. A. Wray, Y. Xia, S.-Y. Xu, M. Z. Hasan, and A. Bansil, *Phys. Rev. B* **82**, 125208 (2010).
- [44] A. Jain, S. P. Ong, G. Hautier, W. Chen, W. D. Richards, S. Dacek, S. Cholia, D. Gunter, D. Skinner, G. Ceder, and K. A. Persson, *APL Materials* **1**, 011002 (2013).
- [45] C. Shi, X. Xi, Z. Hou, X. Zhang, G. Xu, E. Liu, W. Wang, W. Wang, J. Chen, and G. Wu, *physica status solidi (b)* **252**, 357 (2015).
- [46] For $R \in \{Y, Dy, Tb, Sm\}$ in $RPdBi$, the downward curving m_j split Γ_8 bands lies close to the Fermi surface. This can be clearly seen for $YPdBi$ in Refs. [24, 25, 41, 43–45] and for $R \in \{Dy, Tb, Sm\}$ in Ref. [44].
- [47] A. Moreo, M. Daghofer, A. Nicholson, and E. Dagotto, *Phys. Rev. B* **80**, 104507 (2009).
- [48] G. Tang, C. Bruder, and W. Belzig, *Phys. Rev. Lett.* **126**, 237001 (2021).
- [49] J. M. Luttinger and W. Kohn, *Phys. Rev.* **97**, 869 (1955).
- [50] G. Dresselhaus, *Phys. Rev.* **100**, 580 (1955).
- [51] M. Tinkham, *Group Theory and Quantum Mechanics*, Dover Books on Chemistry and Earth Sciences (Dover Publications, 2003).
- [52] M. Dresselhaus, G. Dresselhaus, and A. Jorio, *Group Theory: Application to the Physics of Condensed Matter* (Springer Berlin Heidelberg, 2007).
- [53] See the supplemental information for the details on the folding down approach, power series expansion, band basis formalism, calculation of angular-momentum-resolved

- density of states, detection of the m_j composition of Cooper pairs, spectrum of $j = 3/2$ pairing at FEE and constructing pairing Hamiltonians in cubic point group symmetry. This includes Refs. [6, 8, 9, 15, 20, 42, 51, 52, 54, 64].
- [54] P. Löwdin, *J. Chem. Phys.* **19**, 1396 (1951).
- [55] The analogous model for $(-+)$ subspace can be derived by substituting $(+) \leftrightarrow (-)$ in Eq. (5).
- [56] Due to our choice of the pairing basis, the inter-band gap-like structure $\hat{\delta}(\mathbf{k})$ is proportional to the identity matrix.
- [57] The band crossings of the FEE appear for the C_2 , C_2' , and C_3 axes at $E = \pm 4|\mu\beta/(4\alpha + 5\beta)|$, $E = \pm 2|\mu/(4\alpha + 5\beta)|\sqrt{\beta^2 + 3\gamma^2}$, and $E = \pm 4|\gamma\mu/(4\alpha + 5\beta)|$, respectively. These crossings constitute the prerequisite for the GLSs.
- [58] In the case of low-energy pairing of intra-band electrons, the usual even(odd)-parity pseudo-spin singlet (triplet) as well as the \mathbf{d} -vector representation of the odd-parity states [3, 75] can be deduced from $\hat{\Delta}_{\text{eff}}^{\nu\nu'}(-\mathbf{k}) = -[\hat{\Delta}_{\text{eff}}^{\nu\nu'}(\mathbf{k})]^T$ with $\nu = \nu' \in \{+, -\}$.
- [59] We expand the electron-electron interaction through the orthogonal basis set of cubic point group symmetry. In this regard, the expanded two-body interaction includes many terms each distinguished by the basis label of cubic symmetry and Cooper pair quantum numbers. We investigate each term individually.
- [60] For cubic anisotropy in the normal-state $\gamma \neq \beta$, our results are still valid.
- [61] The pairing channel nomenclature is based on J quantum number of Cooper pairs due to presence of strong spin-orbit coupling.
- [62] There are three (eight) equivalent directions for the proper two(three)-fold rotation $C_{2(3)}$ in cubic point group symmetry. The equivalent directions for the C_2 rotation are $[1, 0, 0]$, $[0, 1, 0]$ and $[0, 0, 1]$. For the C_3 rotation, the equivalent directions are $[1, 1, \bar{1}]$, $[\bar{1}, 1, 1]$, $[1, \bar{1}, 1]$, $[1, 1, \bar{1}]$, $[\bar{1}, \bar{1}, 1]$, $[1, \bar{1}, \bar{1}]$, $[\bar{1}, 1, \bar{1}]$ and $[\bar{1}, \bar{1}, \bar{1}]$, where $\bar{1} \equiv -1$.
- [63] $g(\mathbf{u})$ stands for even(odd)-parity depending on the symmetry of Cooper pair quantum numbers.
- [64] H. Mäkelä and K.-A. Suominen, *Phys. Rev. Lett.* **99**, 190408 (2007).
- [65] W. Yang, T. Xiang, and C. Wu, *Phys. Rev. B* **96**, 144514 (2017).
- [66] In Fig. 2(a), the two-fold degeneracy along the $[0, 0, 1]^*$ direction is not lifted in the presence of inversion breaking ASOC term. This degeneracy is protected by mirror reflection symmetry and can be witnessed in time-reversal symmetric T_d crystals [65].
- [67] E. Bauer and M. Sigrist, Non-Centrosymmetric Superconductors: Introduction and Overview, Lecture Notes in Physics (Springer Berlin Heidelberg, 2012).
- [68] P. A. Frigeri, D. F. Agterberg, A. Koga, and M. Sigrist, *Phys. Rev. Lett.* **92**, 097001 (2004).
- [69] T. Dvir, F. Massee, L. Attias, M. Khodas, M. Aprili, C. H. L. Quay, and H. Steinberg, *Nature Communications* **9**, 598 (2018).
- [70] Y. Okada, Y. Ando, R. Shimizu, E. Minamitani, S. Shiraki, S. Watanabe, and T. Hitosugi, *Nature Communications* **8**, 15975 (2017).
- [71] R. Kumar, A. Vasdev, S. Das, S. Howlader, K. S. Jat, P. Neha, S. Patnaik, and G. Sheet, *Scientific Reports* **11**, 4090 (2021).
- [72] D. Costanzo, H. Zhang, B. A. Reddy, H. Berger, and A. F. Morpurgo, *Nature Nanotechnology* **13**, 483 (2018).
- [73] M. Hashimoto, I. M. Vishik, R.-H. He, T. P. Devereaux, and Z.-X. Shen, *Nature Physics* **10**, 483 (2014).
- [74] S. Kanasugi and Y. Yanase, [arXiv:2107.07096](https://arxiv.org/abs/2107.07096).
- [75] R. Balian and N. R. Werthamer, *Phys. Rev.* **131**, 1553 (1963).

Supplemental Material

CONTENTS

References	4
A. Folding-down approach	7
B. Power series expansion	7
C. Band basis formalism	8
D. Angular-momentum-resolved density of states	8
E. Proposal to detect $j=3/2$ pairing	9
F. Spectrum of $j=3/2$ pairing at finite-excitation energies	11
G. Constructing pairing in O_h symmetry and $j=3/2$ representation	12
1. Symmetry properties of inter-band pairing	13
2. s-wave pairing in O_h symmetry	13
3. p -wave pairing in O_h symmetry	14
a. Singlet state $J=0$	14
b. Triplet state $J=1$	14
c. Quintet state $J=2$	15
d. Septet state $J=3$	15
H. Multipole matrices in $j=3/2$ representation	15

Appendix A: Folding-down approach

In this section, we show the derivation of the effective Hamiltonian presented in Eq. (5) of the Letter through the folding down approach [54]. Consider the following Schrödinger equation

$$\begin{pmatrix} \hat{H}_{11} & \hat{H}_{12} \\ \hat{H}_{21} & \hat{H}_{22} \end{pmatrix} \begin{pmatrix} \hat{\psi}_A \\ \hat{\psi}_B \end{pmatrix} = E \begin{pmatrix} \hat{\psi}_A \\ \hat{\psi}_B \end{pmatrix}, \quad (\text{A1})$$

where \hat{H}_{ij} is a $n \times n$ sub-block matrix and $(\hat{\psi}_A, \hat{\psi}_B)^T$ denotes the eigenvector column with $\hat{\psi}_{A(B)}$ being its sub-block elements. The above eigenvalue problem reduces to the following coupled equations

$$\hat{H}_{11}\hat{\psi}_A + \hat{H}_{12}\hat{\psi}_B = E\hat{\psi}_A, \quad (\text{A2})$$

$$\hat{H}_{21}\hat{\psi}_A + \hat{H}_{22}\hat{\psi}_B = E\hat{\psi}_B. \quad (\text{A3})$$

From Eq. (A3), we obtain $\hat{\psi}_B$ as

$$\hat{\psi}_B = (E\hat{I}_n - \hat{H}_{22})^{-1}\hat{H}_{21}\hat{\psi}_A, \quad (\text{A4})$$

where \hat{I}_n is a $n \times n$ identity matrix. Inserting $\hat{\psi}_B$ into Eq. (A2) results in

$$\hat{\mathcal{H}}_{\text{eff}} \hat{\psi}_A = E\hat{\psi}_A, \quad (\text{A5})$$

where

$$\hat{\mathcal{H}}_{\text{eff}} = \hat{H}_{11} + \hat{H}_{12}(\omega\hat{I}_n - \hat{H}_{22})^{-1}\hat{H}_{21}. \quad (\text{A6})$$

Note that the second term in $\hat{\mathcal{H}}_{\text{eff}}$ has the same basis as \hat{H}_{11} . Moreover, we have taken $E \rightarrow E - \omega + \omega$ where $E - \omega \approx 0$ holds in the vicinity of finite-excitation energies (FEE) ω and making the left hand side of Eq. (A5) independent of E . The effective low-energy pairing can be easily derived by rearranging the inter-band basis of the sub-block Hamiltonians into the intra-band basis as well as setting $\omega \approx 0$.

Appendix B: Power series expansion

Equation (4) of the Letter can be represented in sub-block matrix formalism as

$$\hat{h}_k = \begin{pmatrix} \hat{h}_{11}(\mathbf{k}) & \hat{h}_{12}(\mathbf{k}) \\ \hat{h}_{21}(\mathbf{k}) & \hat{h}_{22}(\mathbf{k}) \end{pmatrix}, \quad (\text{B1})$$

which allows us to employ Eq. (A6). To perform the power series expansion of $(\omega\hat{I}_n - \hat{h}_{22}(\mathbf{k}))^{-1}$, we follow the subsequent steps. Suppose that we are seeking $(\hat{A} + \hat{B})^{-1}$ where \hat{A} and \hat{B} are invertible Hermitian matrices of dimension n . Consider the following identity

$$(\hat{A} + \hat{B})^{-1} = \hat{A}^{-1}(\hat{I}_n + \hat{B}\hat{A}^{-1})^{-1}. \quad (\text{B2})$$

A power series expansion of the right hand side of Eq. (B2) reads

$$\begin{aligned} (\hat{I}_n + \hat{B}\hat{A}^{-1})^{-1} &= \sum_{n=0}^{\infty} (-\hat{B}\hat{A}^{-1})^n \\ &= \hat{I}_n - \hat{B}\hat{A}^{-1} + \mathcal{O}(\hat{B}\hat{A}^{-1})^2. \end{aligned} \quad (\text{B3})$$

Inserting the above expansion into the right hand side of Eq. (B2), this results in

$$(\hat{A} + \hat{B})^{-1} \approx \hat{A}^{-1} - \hat{A}^{-1}\hat{B}\hat{A}^{-1}. \quad (\text{B4})$$

Now, expressing $\omega\hat{I}_n - \hat{h}_{22}(k)$ in terms of normal $\hat{\epsilon}_{\mathbf{k}}$ and pairing $\hat{\Delta}_{\mathbf{k}}$ parts, this results in the following form

$$[\omega\hat{I} - \hat{h}_{22}(\mathbf{k})] = \hat{\epsilon}_{\mathbf{k}} - \hat{\Delta}_{\mathbf{k}}, \quad (\text{B5})$$

with

$$\begin{aligned} \hat{\epsilon}_{\mathbf{k}} &\equiv \begin{pmatrix} (\omega - E_{\mathbf{k}}^-)\hat{\sigma}_0 & 0 \\ 0 & (\omega + E_{\mathbf{k}}^+)\hat{\sigma}_0 \end{pmatrix}, \\ \hat{\Delta}_{\mathbf{k}} &\equiv \begin{pmatrix} 0 & \hat{\Delta}_{\mathbf{k}}^{-+} \\ (\hat{\Delta}_{\mathbf{k}}^{-+})^\dagger & 0 \end{pmatrix}. \end{aligned} \quad (\text{B6})$$

Using Eq. (B4), we arrive immediately at

$$[\omega\hat{I} - \hat{h}_{22}(\mathbf{k})]^{-1} \approx \hat{\mathcal{E}}_{\mathbf{k}}^{-1} + \hat{\mathcal{E}}_{\mathbf{k}}^{-1}\hat{\Delta}_{\mathbf{k}}\hat{\mathcal{E}}_{\mathbf{k}}^{-1}, \quad (\text{B7})$$

where we have assumed that $\hat{\Delta}_{\mathbf{k}}$ in the vicinity of $\tilde{\mathbf{k}}$ is small. Sandwiching the above term between off-diagonal blocks of Eq. (B1), we arrive at

$$\hat{A}(\mathbf{k}) = \hat{h}_{12}(\mathbf{k})[\omega\hat{I} - \hat{h}_{22}(\mathbf{k})]^{-1}\hat{h}_{21}(\mathbf{k}), \quad (\text{B8})$$

which reads explicitly

$$\hat{A}(\mathbf{k}) = \begin{pmatrix} \frac{1}{(\omega+E_{\mathbf{k}}^+)}\Delta_{\mathbf{k}}^{++}(\Delta_{\mathbf{k}}^{++})^\dagger & \frac{1}{\varepsilon_{\mathbf{k}}}\Delta_{\mathbf{k}}^{++}(\Delta_{\mathbf{k}}^{-+})^\dagger\Delta_{\mathbf{k}}^{--} \\ \frac{1}{\varepsilon_{\mathbf{k}}}[\Delta_{\mathbf{k}}^{++}(\Delta_{\mathbf{k}}^{-+})^\dagger\Delta_{\mathbf{k}}^{--}]^\dagger & \frac{1}{(\omega-E_{\mathbf{k}}^-)}(\Delta_{\mathbf{k}}^{-+})^\dagger\Delta_{\mathbf{k}}^{--} \end{pmatrix}, \quad (\text{B9})$$

where $\varepsilon_{\mathbf{k}} = (\omega + E_{\mathbf{k}}^+)(\omega - E_{\mathbf{k}}^-)$. Finally, adding the above term to $\hat{h}_{11}(\mathbf{k})$, this results in Eq. (5) of the Letter. In our choice of time-reversal symmetric pairing, the identity $(\Delta_{\mathbf{k}}^{\nu\nu})^\dagger\Delta_{\mathbf{k}}^{\nu\nu} = \Delta_{\mathbf{k}}^{\nu\nu}(\Delta_{\mathbf{k}}^{\nu\nu})^\dagger$ with $\nu \in \{+, -\}$, holds true since $(\Delta_{\mathbf{k}}^{\nu\nu})^\dagger\Delta_{\mathbf{k}}^{\nu\nu}$ is proportional to the identity matrix.

Appendix C: Band basis formalism

By exact diagonalization of Eq. (1) of the main Letter for the case of SO(3) symmetry, i.e., $\gamma = \beta$, we obtain the eigenvector matrix $\hat{V}_{\mathbf{k}}^\pm$ corresponding to the two-fold degenerate eigenvalues $E_{\mathbf{k}}^\pm$ as

$$\hat{V}_{\mathbf{k}}^+ = \Gamma_{\mathbf{k}}^+ \begin{pmatrix} 2k_z k_- / k_+^2 & k_- / k_+ \\ \sqrt{3}k_- / k_+ & 0 \\ 0 & \sqrt{3} \\ 1 & -2k_z / k_- \end{pmatrix}, \quad (\text{C1})$$

and

$$\hat{V}_{\mathbf{k}}^- = \Gamma_{\mathbf{k}}^- \begin{pmatrix} 2\sqrt{3}k_z k_- (k_x^2 + k_y^2) / k_+^2 & -\sqrt{3}k_-^2 \\ -(k + 3k_z^2)(k_x^2 + k_y^2) / k_+^2 & 0 \\ 0 & k + 3k_z^2 \\ \sqrt{3}(k_x^2 + k_y^2) & 2\sqrt{3}k_z k_+ \end{pmatrix}, \quad (\text{C2})$$

where $\Gamma_{\mathbf{k}}^+ = \sqrt{k_x^2 + k_y^2} / 2k$, $\Gamma_{\mathbf{k}}^- = (2k\sqrt{k + 3k_z^2})^{-1}$, and $k_\pm = k_x \pm ik_y$. Note that the eigenvector matrix $\hat{V} = (\hat{V}_{\mathbf{k}}^+, \hat{V}_{\mathbf{k}}^-)$ is orthonormal (derived by the Gram-Schmidt method) satisfying $\hat{V}^\dagger\hat{V} = \hat{I}_4$. The relation between the band basis (pseudo-spin) operator $\hat{f}_{\mathbf{k}}^\pm$ and the fermionic operator is given by

$$\hat{f}_{\mathbf{k}}^{\pm\dagger} = \hat{c}_{\mathbf{k}}^\dagger \hat{V}_{\mathbf{k}}^\pm. \quad (\text{C3})$$

The band basis operators should transform under time-reversal and inversion operations as usual fermionic operators. To construct such correspondence, we act with the anti-unitary time-reversal operation Θ on the fermionic basis $c_{\mathbf{k},m}$ in the usual way

$$\Theta c_{\mathbf{k},m_j} = (-1)^{j+m_j} c_{-\mathbf{k},-m_j}, \quad (\text{C4})$$

where the electron annihilation operator acquires a phase in addition to a sign change of momentum and magnetic quantum number m_j . To perform the above operation on the basis of the normal state Hamiltonian $\hat{c}_{\mathbf{k},m} = (c_{\mathbf{k},3/2}, c_{\mathbf{k},1/2}, c_{\mathbf{k},-1/2}, c_{\mathbf{k},-3/2})^T$, we introduce the matrix representation of the time-reversal operator in $j = 3/2$ basis as $\hat{\Theta} = \hat{\mathcal{T}}\mathcal{K}$ with $\hat{\mathcal{T}} = i\hat{\sigma}_x \otimes \hat{\sigma}_y$ and \mathcal{K} being the unitary part of the time-reversal operator and the complex conjugate operator, respectively. Therefore, the time-reversal transformation of the normal-state basis takes the form

$$\hat{\mathcal{T}}^{-1}\hat{c}_{\mathbf{k}} = \hat{c}'_{-\mathbf{k}}, \quad (\text{C5})$$

where $\hat{c}'_{-\mathbf{k}}$ is the column of time-reversed fermionic operators given by

$$\hat{c}'_{-\mathbf{k}} = (-c_{-\mathbf{k},-3/2}, c_{-\mathbf{k},-1/2}, -c_{-\mathbf{k},1/2}, c_{-\mathbf{k},3/2})^T. \quad (\text{C6})$$

Note that $\hat{\mathcal{T}}$ fulfills the property $\hat{\mathcal{T}}^2 = -\hat{I}_4$. Also, the pseudo-spin operator $\hat{f}_{\mathbf{k},\uparrow\downarrow}$ under time-reversal operation obeys Eq. (C4) as

$$\hat{\mathcal{T}}^{-1}\hat{f}_{\mathbf{k}}^\pm = \hat{f}'_{-\mathbf{k}}^\pm, \quad (\text{C7})$$

with $\hat{\mathcal{T}} = i\hat{\sigma}_y$ denoting the 2×2 matrix representation of the unitary part of the time-reversal operator in pseudo-spin-1/2 basis, and

$$\hat{f}'_{-\mathbf{k}}^\pm = (-f_{-\mathbf{k},\downarrow}^\pm, f_{-\mathbf{k},\uparrow}^\pm). \quad (\text{C8})$$

Note that we have taken into account the pseudo-spin index as effective spin-1/2 index. Inserting Eqs. (C7) into Eq. (C5), this results in

$$V'_{-\mathbf{k}} = -\hat{\mathcal{T}}V_{\mathbf{k}}^*(i\sigma_y), \quad (\text{C9})$$

with $V'_{-\mathbf{k}}$ being the time-reversed matrix of eigenvectors. Moreover, the band basis operators satisfy inversion symmetry as $\hat{V}_{\mathbf{k}}^\pm = \hat{V}'_{-\mathbf{k}}$.

Appendix D: Angular-momentum-resolved density of states

In this section, we derive the angular-momentum-resolved density of states (DOS) in the BdG formalism for $j = 3/2$ superconductors. Consider the Luttinger model in the superconducting phase described by the BdG Hamiltonian in Eq. (3) of the Letter. Diagonalizing the superconducting Hamiltonian $H = \sum_{\mathbf{k}} \hat{\psi}_{\mathbf{k}}^\dagger \hat{H}_{\text{BdG}}(\mathbf{k}) \hat{\psi}_{\mathbf{k}}$, this results in

$$H = \sum_{\mathbf{k}} \hat{a}_{\mathbf{k}}^\dagger \hat{\mathbb{E}}_{\mathbf{k}} \hat{a}_{\mathbf{k}}, \quad (\text{D1})$$

with the basis

$$\hat{a}_{\mathbf{k}}^\dagger = (a_{\mathbf{k},1}^\dagger, a_{\mathbf{k},2}^\dagger, a_{\mathbf{k},3}^\dagger, a_{\mathbf{k},4}^\dagger, a_{\mathbf{k},5}^\dagger, a_{\mathbf{k},6}^\dagger, a_{\mathbf{k},7}^\dagger, a_{\mathbf{k},8}^\dagger), \quad (\text{D2})$$

where $a_{\mathbf{k},i}^\dagger$ is the creation operator for BdG quasi-particles of the i th excitation band and $\hat{\mathbb{E}}_{\mathbf{k}} = \hat{U}_{\mathbf{k}}^\dagger \hat{H}_{\text{BdG}}(\mathbf{k}) \hat{U}_{\mathbf{k}}$ is a 8×8 diagonal matrix of eigenvalues, with $\hat{U}_{\mathbf{k}}$ the matrix of eigenspinors, given by

$$\hat{\mathbb{E}}_{\mathbf{k}} = \text{diag}(E_{\mathbf{k},1}, E_{\mathbf{k},2}, E_{\mathbf{k},3}, E_{\mathbf{k},4}, E_{\mathbf{k},5}, E_{\mathbf{k},6}, E_{\mathbf{k},7}, E_{\mathbf{k},8}). \quad (\text{D3})$$

The relationship between the basis of the Hamiltonian and its band basis (eigenbasis) is given by $\hat{a}_{\mathbf{k}}^\dagger = \hat{\psi}_{\mathbf{k}}^\dagger \hat{U}_{\mathbf{k}}$ with

$$\hat{U}_{\mathbf{k}} = (\hat{\Phi}_{\mathbf{k},1}, \hat{\Phi}_{\mathbf{k},2}, \hat{\Phi}_{\mathbf{k},3}, \hat{\Phi}_{\mathbf{k},4}, \hat{\Phi}_{\mathbf{k},5}, \hat{\Phi}_{\mathbf{k},6}, \hat{\Phi}_{\mathbf{k},7}, \hat{\Phi}_{\mathbf{k},8}), \quad (\text{D4})$$

where $\hat{\Phi}_{\mathbf{k},i}$ is the eigenspinor corresponding to $E_{\mathbf{k},i}$ with $i = \{1, 2, 3, 4, 5, 6, 7, 8\}$ being the band indices. Each $\hat{\Phi}_{\mathbf{k},i}$ is comprised of electron (e) and hole (h) probability weights denoted by $\hat{\Phi}_{\mathbf{k},i} = (\hat{\Phi}_{\mathbf{k},i}^e, \hat{\Phi}_{\mathbf{k},i}^h)^T$. The electron (hole) components are given by

$$\hat{\Phi}_{\mathbf{k},i}^{e(h)} = (u_{\mathbf{k},i,\frac{3}{2}}^{e(h)}, u_{\mathbf{k},i,\frac{1}{2}}^{e(h)}, u_{\mathbf{k},i,-\frac{1}{2}}^{e(h)}, u_{\mathbf{k},i,-\frac{3}{2}}^{e(h)}). \quad (\text{D5})$$

In Eq. (D5), the components are labeled by the magnetic quantum number $m_j = \pm 3/2, \pm 1/2$ due to the choice of basis. According to the above description, the angular-momentum-resolved DOS in the BdG formalism takes the form

$$N_{m_j}(E) = \sum_{i=1}^N \sum_{\mathbf{k}} \delta(E - E_{\mathbf{k},i}) (|u_{\mathbf{k},m_j}^e|^2 + |u_{\mathbf{k},m_j}^h|^2), \quad (\text{D6})$$

with $N = 8$ being the total number of excitation energy bands. The total superconducting DOS can be derived by taking into account the contribution of all m_j components of the DOS given by

$$N(E) = \sum_{m_j} N_{m_j}(E) = \sum_{i=1}^N \sum_{\mathbf{k}} \delta(E - E_{\mathbf{k}}^i), \quad (\text{D7})$$

where $m_j \in \{3/2, 1/2, -1/2, -3/2\}$. Eq. (D7) is simplified due to normalization condition

$$\sum_{m_j} (|u_{\mathbf{k},m_j}^e|^2 + |u_{\mathbf{k},m_j}^h|^2) = 1. \quad (\text{D8})$$

Appendix E: Proposal to detect $j = 3/2$ pairing

To address the observability of the m_j structure of $j = 3/2$ Cooper pairing, we propose to investigate the m_j -resolved DOS in the presence of a perturbative Zeeman field. The corresponding term in the Hamiltonian is given by $\hat{B} = \mathcal{M} \cdot \hat{\mathbf{J}}$ with $\mathcal{M} = (\mathcal{M}_x, \mathcal{M}_y, \mathcal{M}_z)$ being

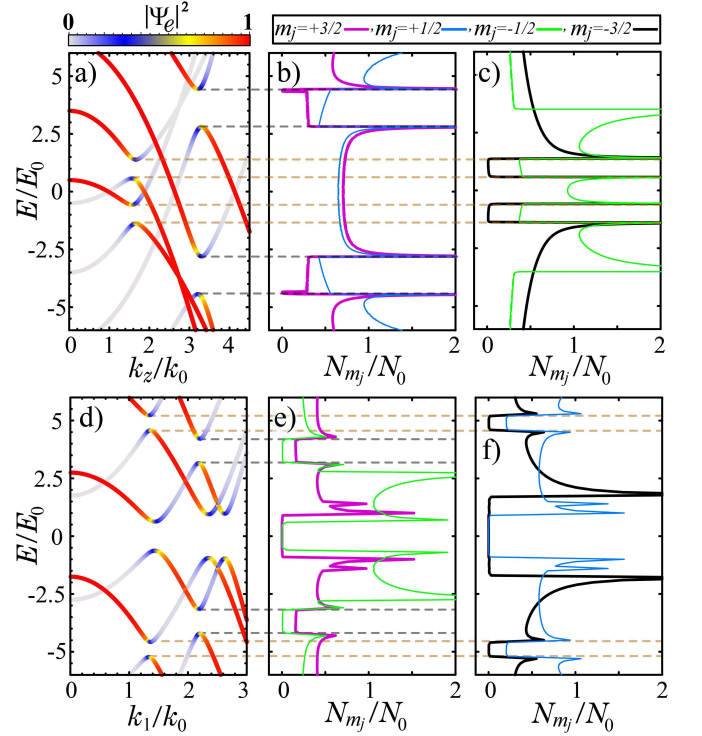


Fig. 3. Superconducting spectra of the p-wave septet pairing in (a) $[0, 0, 1]$ and (d) $[1, 1, 0]$ (i.e., $k_x = k_y = k_1$ and $k_z = 0$) directions for parameters (a) $(\Delta/E_0 a, \delta/E_0 a, m_z/E_0) = (3, 0, 3)$ and (d) $(\Delta/E_0 a, \delta/E_0 a, m_z/E_0) = (4, 0.5, 4.5)$, respectively. The color denotes the probability of electronic states $|\Psi_e|^2$ in panels (a) and (d). The m_j -resolved DOS of panel (a) [(d)] is depicted in panels (b) and (c) [(e) and (f)]. Other parameters are $\mu/E_0 = -5$, $k_0 = 0.1a^{-1}$, $E_0 = 10^{-2}|\alpha|a^{-2}$, $\beta = 0.2|\alpha|$, $\gamma = -0.05|\alpha|$, $\alpha = -20$, and $N_0 = 10^5$.

the Zeeman vector and $\hat{\mathbf{J}} = (\hat{J}_x, \hat{J}_y, \hat{J}_z)$ defining the vector of $j = 3/2$ matrices. The doubly degenerate energy bands have zero net magnetization throughout momentum space due to the combination of time-reversal and inversion symmetries. In the presence of the Zeeman field, the energy bands incorporating states with different magnetic quantum number m_j are split as a consequence of time reversal symmetry breaking and they acquire finite magnetization.

Without loss of generality, we choose the magnetic field to point in z direction, i.e., $\mathcal{M} = (0, 0, \mathcal{M}_z)$. We focus on the p-wave septet pairing channel since this is the most energetically favorable instability channel in half-Heusler materials with T_d crystalline structure [42]. For a finite value of \mathcal{M}_z , the spectrum in Fig. 1(c) of the Letter is re-plotted in Fig. 3(a) below in the presence of cubic anisotropy. The m_j -resolved DOS, according to Eq. (D6), is depicted in Fig. 3(b) and (c). The solid lines with magenta, light blue, light green and black colors illustrate $N_{3/2}(E)$, $N_{1/2}(E)$, $N_{-1/2}(E)$ and $N_{-3/2}(E)$, respectively.

Fig. 3(a) shows that the nodal behavior at low-energy is remained intact while a pair of GLSs, shown in Fig. 1(c) of the Letter, are split into two pairs of GLSs due to violation of time-reversal symmetry. We point out that the larger GLSs happen within the excitation energy ranges $E/E_0 \in [2.8, 4.4]$ and $E/E_0 \in [-4.4, -2.8]$. Interestingly, in this energy range, the simultaneous abrupt drops of the m_j -resolved DOS in Fig. 3(b) signal hybridization of electrons with different quantum numbers, i.e., $m_j = 3/2$ with $m_j = 1/2$. To visualize it, we connect the GLSs energy range in Fig. 3(a) to the energy range of coherence peaks in Fig. 3(b) with gray dashed lines. In addition, the smaller GLSs appearing in the energy ranges $E/E_0 \in [0.55, 1.35]$ and $E/E_0 \in [-1.35, -0.55]$ stem from superconducting hybridization of $m_j = -3/2$ and $m_j = -1/2$ states. This is signaled by simultaneous drops of $N_{-3/2}(E)$ and $N_{-1/2}(E)$ in these energy regions (light brown dashed lines) as shown in Fig. 3(c). Surprisingly, the DOS of $m_j = -3/2$ states completely vanishes at FEE. This is because the $m_j = -3/2$ electron band is located below the hybridization energy $E(\tilde{k})$ where pairing occur with $m_j = -1/2$ states. In this case, there are no states within the GLS excitation energies as illustrated in Fig. 4(a) where the dashed lines mark the paired area. This converts the superconducting GLS into a *full gap* for a particular choice of m_j at finite-energies despite of having multiband structure. The DOS $N_{-3/2}(E)$ in Fig. 3(c) corresponds to the $m_j = -3/2$ resolved spectrum in Fig. 4(a). Note also that the m_j -resolved DOS in Fig. 3(b) and (c) show finite values at $E = 0$ due to the nodal behavior.

The observation of m_j -resolved DOS is challenging, but keeping in mind to role of multiband systems in modern quantum materials. In principle, it can be accomplished in a similar way as spin-resolved spectroscopy. We need a spectrometer (e.g. based on scanning tunneling spectroscopy) that is able to distinguish electrons with different magnetic quantum numbers. We may ask about the reason behind the superconducting hybridization of states with *equal sign* of m_j in the aforementioned example. The reason is rooted in the anisotropy of the instability channel in momentum space, in which the paired states with different m_j are affected by the wave vector. Due to the absence of ASOC, j_z is conserved along the z -axis and it is instructive to look at the second quantization representation of the pairing channel given by Eq. (G30) below as $H_{xyz}^{3,3,1} = \sum_{k_z} \hat{c}_{k_z}^\dagger \hat{H}_{xyz}^{3,3,1}(k_z) \hat{c}_{-k_z}^\dagger$ which can be written as

$$H_{xyz}^{(3,3,1)} = \frac{\sqrt{3}}{2} \Delta \sum_{k_z} k_z (c_{\frac{3}{2}}^\dagger c_{\frac{1}{2}}^\dagger + c_{\frac{1}{2}}^\dagger c_{\frac{3}{2}}^\dagger + c_{-\frac{3}{2}}^\dagger c_{-\frac{1}{2}}^\dagger + c_{-\frac{1}{2}}^\dagger c_{-\frac{3}{2}}^\dagger) + h.c., \quad (\text{E1})$$

where the momentum dependency of the operators are dropped for ease of notation. According to Eq. (E1), we can realize that the pair operators with different m_j

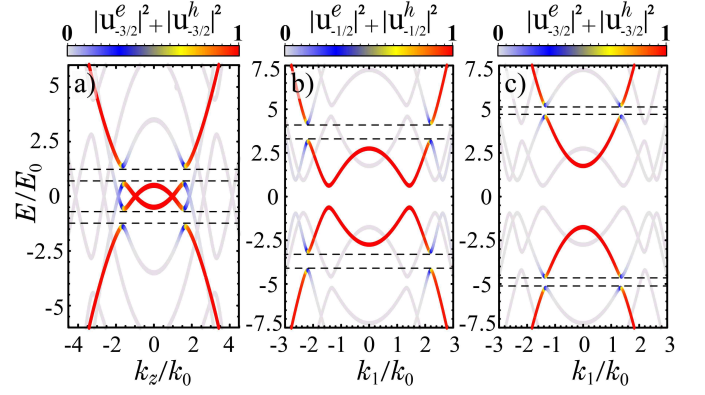


Fig. 4. Angular-momentum-resolved BdG spectra of the p-wave septet pairing in (a) $[0, 0, 1]$ and (b,c) $[1, 1, 0]$ (i.e., $k_x = k_y = k_1$ and $k_z = 0$) directions. The color bar denotes the probability weights of quasi-particles with (a) $m_j = -3/2$, (b) $m_j = -1/2$ and (c) $m_j = -3/2$ magnetic quantum number. Other parameters are the same as those in Fig. 3.

and *equal* signs remain finite along the z -direction due to the anisotropic form of the pairing channel. Importantly, the larger (smaller) GLSs in Fig. 3(b) [(c)] correspond to $c_{3/2}^\dagger c_{1/2}^\dagger + c_{1/2}^\dagger c_{3/2}^\dagger$ ($c_{-1/2}^\dagger c_{-3/2}^\dagger + c_{-3/2}^\dagger c_{-1/2}^\dagger$) pairing operators. Note that the presence of nodal degeneracies at low energies are due to the absence of pairing between states with identical m_j .

It is important to mention that the resolution of superconducting coherence peaks in quantum numbers m_j is restricted neither to the $[0, 0, 1]$ direction nor the conservation of j_z . To show this, we focus on the C'_2 axis, i.e., $[1, 1, 0]$ direction, where the conservation of j_z is violated due to the presence of symmetric and antisymmetric spin-orbit coupling. The spectrum, in the presence of a perpendicular magnetic field $m_z = 4.5E_0$ and a small value of ASOC, is calculated in Fig. 3(d). The split GLSs with larger partial band gap correspond to pairing of $m_j = 3/2$ and $m_j = -1/2$ states according to the coincident drops of $N_{m_j}(E)$ in Fig. 3(e). The corresponding energy range is enclosed by gray dashed lines. Remarkably, $N_{-1/2}(E)$ vanishes completely at FEE owing to the fact that the $m_j = -1/2$ electron band is pushed below the superconducting energy $E(\tilde{k})$ as a consequence of interplay between magnetic field and Fermi energy. The corresponding $m_j = -1/2$ resolved spectra having zero DOS character (Fig. 3(e)) is plotted in Fig. 4(b) where the full superconducting gap at FEE is illustrated between the dashed lines. Moreover, the smaller GLSs in Fig. 3(d) are composed by pairing of $m_j = -3/2$ and $m_j = 1/2$ states according to Fig. 3(f) with entirely vanishing $N_{-3/2}(E)$ at FEE. The reason of $N_{-3/2}(E)$ disappearance is the same as we explained earlier and the $m_j = -3/2$ resolved excitations are depicted in Fig. 4(c).

Interestingly, we find that novel Cooper pairs possessing larger magnetic quantum numbers exhibit larger

GLSs in the presence of magnetic fields. To show this, we identify the total magnetic quantum number of a *local* finite-energy Cooper pair. We should represent the two-particle state $|j_1, j_2; m_{j_1}, m_{j_2}\rangle \equiv |m_{j_1}, m_{j_2}\rangle$ into a local pair state $|\mathcal{J}, m_{\mathcal{J}}\rangle$ given by

$$|m_{j_1}, m_{j_2}\rangle = \sum_{\mathcal{J}, m_{\mathcal{J}}} \langle \mathcal{J}, m_{\mathcal{J}} | m_{j_1}, m_{j_2} \rangle |\mathcal{J}, m_{\mathcal{J}}\rangle, \quad (\text{E2})$$

where $\langle \mathcal{J}, m_{\mathcal{J}} | m_{j_1}, m_{j_2} \rangle$ denotes the Clebsch-Gordan coefficient (CGC), $j_1 = j_2 = 3/2$ due to the high-angular momenta nature of the Γ_8 bands, and \mathcal{J} indicates the total angular momentum of a local Cooper pair with relative magnetic quantum number $m_{\mathcal{J}}$. The ‘‘local’’ term points to those energy bands with distinct indices contributing to pairing among all the energy bands. For instance, according to Figs. 3(b) and (c), the larger GLSs in Fig. 3(b) correspond to Cooper pairing formed by single-particle state with quantum numbers $m_j = 3/2$ and $m_j = 1/2$ as

$$|\frac{3}{2}, \frac{1}{2}\rangle + |\frac{1}{2}, \frac{3}{2}\rangle \propto |\mathcal{J} = 3, m_{\mathcal{J}} = 2\rangle. \quad (\text{E3})$$

Likewise, the smaller GLSs in Fig. 3(c) correspond to Cooper pairing with quantum numbers

$$|-\frac{3}{2}, -\frac{1}{2}\rangle + |-\frac{1}{2}, -\frac{3}{2}\rangle \propto |\mathcal{J} = 3, m_{\mathcal{J}} = -2\rangle. \quad (\text{E4})$$

From Eqs. (E3) and (E4), we confirm that the exotic pairings have septet total angular momentum $\mathcal{J} = 3$ with $m_{\mathcal{J}} = 2$ and $m_{\mathcal{J}} = -2$ magnetic quantum numbers signaled by the larger and smaller GLSs, respectively.

It is worthwhile to mention that the above results do not rely on the model parameters. They are not even restricted to special directions in momentum space. The physics remains valid within the entire momentum space and applies to other pairing channels.

Appendix F: Spectrum of $j = 3/2$ pairing at finite-excitation energies

In this section, we present two examples to elucidate the effective non-BdG two-band model given in Eq. (7) of the Letter. The model captures superconducting spectrum close to GLS at FEE. We start by focusing on the p-wave septet pairing to calculate $\text{Tr}(\hat{\varepsilon}_{\mathbf{k}}^{\nu\nu}) = \frac{1}{2}\text{Tr}(\hat{\Delta}_{\mathbf{k}}^{\nu\nu}(\hat{\Delta}_{\mathbf{k}}^{\nu\nu})^\dagger)/(\omega + \nu E_{\mathbf{k}}^\nu)$ for doubly degenerate bands given by indices $\nu \in \{+, -\}$. For simplicity, we assume $\gamma = \beta$ resulting in the normal state spectra $E_{\mathbf{k}}^+ = (\alpha + 9\beta/4)k^2 - \mu$ and $E_{\mathbf{k}}^- = (\alpha + \beta/4)k^2 - \mu$. In this case, we have

$$\frac{1}{2}\text{Tr}(\hat{\Delta}_{\mathbf{k}}^{++}(\hat{\Delta}_{\mathbf{k}}^{++})^\dagger) = 81\Delta_{\mathbf{k}}^2(k_x^2 + k_y^2)(k_x^2 + k_z^2)(k_y^2 + k_z^2), \quad (\text{F1})$$

$$\frac{1}{2}\text{Tr}(\hat{\Delta}_{\mathbf{k}}^{--}(\hat{\Delta}_{\mathbf{k}}^{--})^\dagger) = 9\Delta_{\mathbf{k}}^2(k_x^4(k_y^2 + k_z^2) + k_y^4(k_x^2 + k_z^2) + k_z^4(k_x^2 + k_y^2) - 6k_x^2k_y^2k_z^2), \quad (\text{F2})$$

$$\hat{\delta}(\mathbf{k}) = 3\Delta_{\mathbf{k}}^2(4(k_x^6 + k_y^6 + k_z^6) - 3[k_x^4(k_y^2 + k_z^2) + k_y^4(k_x^2 + k_z^2) + k_z^4(k_x^2 + k_y^2) - 2k_x^2k_y^2k_z^2]), \quad (\text{F3})$$

with $\Delta_{\mathbf{k}} = (\Delta/4k)^2$. Note that Eq. (F1) (Eq. (F2)) indicates the magnitude of low-energy Cooper pairing composed by two intra-band electrons having identical magnetic quantum numbers $m_j = 3/2$ ($m_j = 1/2$).

We derive the non-BdG two-band spectra corresponding to Figs. 1(c) and (d) of the Letter. The low-energy pairing vanishes along $[0, 0, 1]$ direction leading to $\text{Tr}(\hat{\varepsilon}_{\mathbf{k}}^{++}) = \text{Tr}(\hat{\varepsilon}_{\mathbf{k}}^{--}) = 0$. Also, the finite-energy pairing becomes $\hat{\delta}(\mathbf{k}) = 3\Delta^2k_z^2/4$. Consequently, the FEE spectrum takes the form

$$\mathcal{E}_{\pm}(k_z) = \beta k_z^2 \pm \sqrt{\frac{\vartheta^2}{16}k_z^4 - \frac{\vartheta\mu}{2}k_z^2 + \mu^2 + \frac{3}{4}k_z^2\Delta^2}, \quad (\text{F4})$$

with $\vartheta = 4\alpha + 5\beta$. Eq. (F4) denotes the exotic pair-

ing occurring for positive excitation energies as shown in Fig. 5(b). The vertical dashed line indicates $k_z = \tilde{k} = 2\sqrt{\mu/(4\alpha + 5\beta)}$ where pairing between $m_j = 3/2$ and $m_j = 1/2$ electrons happen. We can witness in Fig. 5(b) that the GLS happening at $k_z = \tilde{k}$ is in an excellent agreement with the spectrum derived directly by the BdG Hamiltonian in Fig. 5(a). Likewise, the GLS below the Fermi level is plotted in Fig. 5(c). In both panels (b) and (c), the particle-hole symmetry is broken due to presence of non-identical diagonal entries, *cf.* Eq. (5) of the Letter.

Furthermore, the low-energy pairing along the $[1, 1, 0]$ direction in both energy bands is finite leading to two superconducting gaps at the Fermi surface as shown in

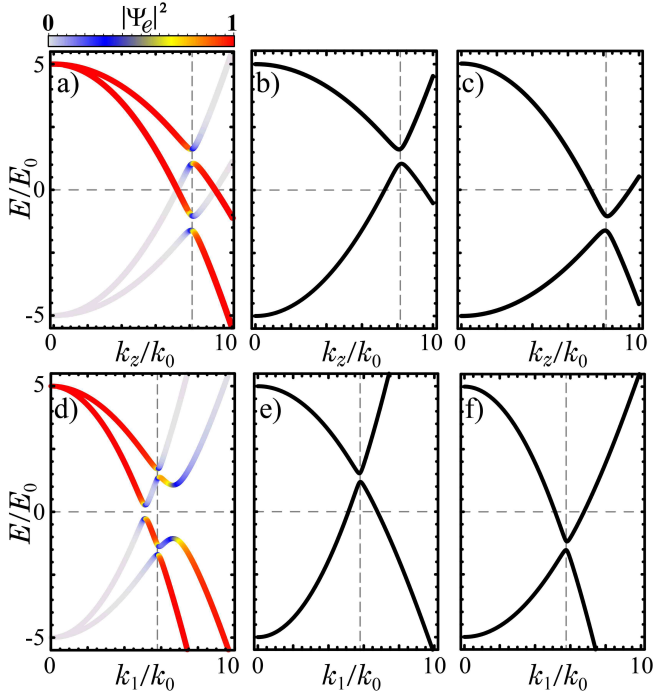


Fig. 5. BdG spectra (a) and (d) resemble to those in Figs. 1(c) and 1(d) in the Letter, respectively. The right panels (b) and (c) [(e) and (f)] denote the non-BdG effective spectra calculated by Eq. (7) of the Letter to capture FEE pairing. The pairing strength is (a) $\Delta/E_0 a = 4.15$ (b) $\Delta/E_0 a = 10$. Other parameters are $\beta = 0.2|\alpha|$, $\gamma = \beta$, $\mu/E_0 = -5$, $k_0 = 10^{-2}a^{-1}$, $E_0 = 10^{-3}|\alpha|a^{-2}$, and $\alpha = -20$. The vertical dashed lines indicate the exotic pairing momentum for (a) $\tilde{k} = 2\sqrt{\mu/(4\alpha + 5\beta)}$ and (d) $\tilde{k} = \sqrt{2\mu/(4\alpha + 5\beta)}$. The horizontal line denotes the Fermi surface.

Fig. 5(d). To capture the exotic superconducting GLS at FEE, the contribution of low-energy pairing induces a pseudospin energy shift given by $(1/2)\text{Tr}(\hat{\Delta}_{\mathbf{k}}^{++}(\hat{\Delta}_{\mathbf{k}}^{++})^\dagger) = (81/32)k^2\Delta^2$ and $(1/2)\text{Tr}(\hat{\Delta}_{\mathbf{k}}^{--}(\hat{\Delta}_{\mathbf{k}}^{--})^\dagger) = (9/32)k^2\Delta^2$. Taking into account these shifts, the non-BdG spectrum for GLS above and below $E = 0$ are shown in Figs. 5(e) and (f), respectively. In this case, the exotic GLSs appear at $k_1 = \tilde{k} = \sqrt{2\mu/(4\alpha + 5\beta)}$. Taking into account the pseudospin energy shifts, the excitation behaviors around GLSs are consistent with full BdG spectrum in Fig. 5(d).

Appendix G: Constructing pairing in O_h symmetry and $j=3/2$ representation

We start by the density-density interaction decomposed in the pair scattering formalism with the total intrinsic spin S in the $j = 3/2$ basis as

$$H_V = \sum_{\mathbf{k}, \mathbf{k}'} \sum_{S, m_S} V(\mathbf{k} - \mathbf{k}') b_{S, m_S}^\dagger(\mathbf{k}) b_{S, m_S}(\mathbf{k}'), \quad (\text{G1})$$

where $b_{S, m_S}^\dagger(\mathbf{k})$ [$b_{S, m_S}(\mathbf{k}')$] creates (annihilates) a Cooper pair with intrinsic angular momentum S and

spin magnetic quantum number m_S . The correspondence between the Cooper pair operator and the two-electron state is given by

$$b_{S, m_S}^\dagger(\mathbf{k}) = \sum_{m_{j_1}, m_{j_2}} \langle j_1, j_2; m_{j_1}, m_{j_2} | S, m_S \rangle c_{\mathbf{k}, m_{j_1}}^\dagger c_{-\mathbf{k}, m_{j_2}}^\dagger, \quad (\text{G2})$$

where $\langle j_1, j_2; m_{j_1}, m_{j_2} | S, m_S \rangle$ is the CGC connecting the two-electron state $|j_1, j_2; m_{j_1}, m_{j_2}\rangle \equiv c_{\mathbf{k}, m_{j_1}}^\dagger c_{-\mathbf{k}, m_{j_2}}^\dagger |0\rangle$ with the Cooper pair state $|S, m_S\rangle = b_{S, m_S}^\dagger(\mathbf{k}) |0\rangle$ in intrinsic total spin representation. Here, each electron has total angular momentum j with relative magnetic quantum number m_j . For convenience, we can represent the Cooper pair operator in a compact form with the aid of spin multipole matrices [8, 9, 15] as

$$\begin{aligned} b_{S, m_S}^\dagger(\mathbf{k}) &= \hat{c}_{\mathbf{k}}^\dagger [\hat{S}_{S, m_S} \hat{T}] (\hat{c}_{-\mathbf{k}}^\dagger)^T, \\ b_{S, m_S}(\mathbf{k}') &= (\hat{c}_{-\mathbf{k}'}^T)^\dagger [\hat{S}_{S, m_S} \hat{T}]^\dagger \hat{c}_{\mathbf{k}'}, \end{aligned} \quad (\text{G3})$$

where \hat{T} plays the role of Cooper pair symmetrization and anti-symmetrization, and \hat{S}_{S, m_S} denotes the rank-3 spherical spin multipole matrices corresponding to the $j = 3/2$ representation. Note that the \hat{S}_{S, m_S} have the properties of spin multipole moments since Cooper pairs are formed with two charges. Hence, they can be classified as spin dipole, quadrupole, octupole moments, etc for $S = 1, 2, 3, \dots$, respectively. By comparing Eqs. (G2) and (G3), we can conclude that $\hat{S}_{S, m_S} \hat{T}$ is the matrix of CGCs relating the single particle Cooper pair state to the two electron state. Therefore, to derive the multipole matrices, we must find the highest weight matrix by setting $m_S = S$ and $\hat{S}_{S, S} = \hat{C}_{S, S} \hat{T}^{-1}$ where $\hat{C}_{S, S}$ is the matrix composed of CGCs. Then, the lower weight spin multipole matrices can be computed by the recursive formula $[\hat{S}_-, \hat{S}_{S, m_S}] = \hbar \sqrt{S(S+1) - m_S(m_S-1)} \hat{S}_{S, m_S-1}$ where $\hat{S}_- = \hat{S}_x - i\hat{S}_y$. Furthermore, the interaction potential $V(\mathbf{k} - \mathbf{k}')$ can be expanded in terms of spherical harmonics

$$V(\mathbf{k} - \mathbf{k}') = \sum_{L, m_L} \frac{\alpha_L(\mathbf{k}, \mathbf{k}')}{2L+1} Y_{L, m_L}(\mathbf{k}) Y_{L, m_L}^*(\mathbf{k}'). \quad (\text{G4})$$

where the orbital axial angular momentum satisfies the condition $-L \leq m_L \leq L$ and the coefficient $\alpha_L(\mathbf{k}, \mathbf{k}')$ can be derived by $\alpha_L(\mathbf{k}, \mathbf{k}') = \int d\Omega \int d\Omega' \sum_{m_{L'}} Y_{L, m_{L'}}^*(\mathbf{k}) Y_{L', m_{L'}}(\mathbf{k}') V(\mathbf{k} - \mathbf{k}')$. Here, \mathbf{k} denotes the norm of momentum vector. Note that the orthogonality of spherical harmonics implies $\int d\Omega Y_{L, m_L}^*(\mathbf{k}) Y_{L, m_L}(\mathbf{k}) = \delta_{L, L'} \delta_{m_L, m_{L'}}$, where $d\Omega = \sin(\theta) d\theta d\varphi$. Inserting Eqs. (G3) and (G4) into Eq. (G1), this results in the interaction Hamiltonian in the representation of $SO(3)$ symmetry

$$\begin{aligned} H_V^{(L, S)} &= \sum' \left[\hat{c}_{\mathbf{k}}^\dagger (Y_{L, m_L}(\mathbf{k}) \hat{S}_{S, m_S} \hat{T}) (\hat{c}_{-\mathbf{k}}^\dagger)^T \right] \times \\ &\quad \left[(\hat{c}_{-\mathbf{k}'}^T)^\dagger (Y_{L, m_L}(\mathbf{k}') \hat{S}_{S, m_S} \hat{T})^\dagger \hat{c}_{\mathbf{k}'} \right], \end{aligned} \quad (\text{G5})$$

where $\sum' = \sum_{\mathbf{k}, \mathbf{k}'} \sum_{S, m_S} \sum_{L, m_L} [\alpha_L(\mathbf{k}, \mathbf{k}') / (2L + 1)]$. In our system, the total angular momentum J is a good quantum number due to presence of strong spin-orbit coupling. Thus, the density-density interaction in Eq. (G5) should be decomposed in the irreducible representation of total angular momentum. Therefore, the function matrices $Y_{L, m_L}(\mathbf{k}) \hat{\mathcal{S}}_{S, m_S}$ can be transformed into the total angular momentum J basis by $Y_{L, m_L}(\mathbf{k}) \hat{\mathcal{S}}_{S, m_S} = \sum_{J, m_J} \langle J, m_J | m_L, m_S \rangle \hat{\mathcal{N}}_{J, m_J}^{S, L}(\mathbf{k})$ where $\langle J, m_J | m_L, m_S \rangle$ denotes the CGC connecting the Ket $|L, S; m_L, m_S\rangle = |L, m_L\rangle \otimes |S, m_S\rangle$ with the Bra $\langle J, m_J|$. Note that the $\hat{\mathcal{N}}_{J, m_J}^{S, L}(\mathbf{k})$ indicates the total angular momentum multipole matrices. Eventually, we arrive at the density-density interaction in the representation of J as

$$H_V^{(J, S, L)} = \sum'' \left[\hat{c}_{\mathbf{k}}^\dagger (\hat{\mathcal{N}}_{J, m_J}^{S, L}(\mathbf{k}) \hat{\mathcal{T}}) (\hat{c}_{-\mathbf{k}}^\dagger)^T \right] \times \left[(\hat{c}_{-\mathbf{k}'}^T)^T (\hat{\mathcal{N}}_{J, m_J}^{S, L}(\mathbf{k}') \hat{\mathcal{T}})^\dagger \hat{c}_{\mathbf{k}'} \right], \quad (\text{G6})$$

where $\sum'' = \sum_{\mathbf{k}, \mathbf{k}'} \sum_{J, m_J} \sum_{S, L} [\alpha_L(\mathbf{k}, \mathbf{k}') / (2L + 1)]$ and

$$\hat{\mathcal{N}}_{J, m_J}^{S, L}(\mathbf{k}) = \sum_{m_L, m_S} \langle m_L, m_S | J, m_J \rangle Y_{L, m_L}(\mathbf{k}) \hat{\mathcal{S}}_{S, m_S}. \quad (\text{G7})$$

This filters out magnetic orbital and axial spin angular momenta satisfying $|m_L + m_S| = m_J$. Note that for $L = 1$, we have $\alpha_{L=1} = 4\pi|\mathbf{k}||\mathbf{k}'|$.

In the presence of spherical symmetry, the gap functions are labeled by an infinite number of IRs corresponding to $SO(3)$ symmetry, i.e., the total angular momentum J . However, crystals with cubic point group structure have lower symmetry. Therefore, the corresponding pairing instabilities and the corresponding Cooper pair operator must be labeled by the IRs of O_h symmetry. Thus, we need to derive the cubic representation of $\hat{\mathcal{N}}_{J, m_J}^{S, L}(\mathbf{k})$. This can be done by the following relation [20]

$$\hat{\mathcal{N}}_{\eta}^{J, S, L}(\mathbf{k}) = \sum''' (\hat{\mathcal{O}}_{\eta} \hat{\mathcal{T}})_{m_{j_1}, m_{j_2}} \langle m_{j_1}, m_{j_2} | J, m_J \rangle \hat{\mathcal{N}}_{J, m_J}^{S, L}(\mathbf{k}), \quad (\text{G8})$$

where $\sum''' = \sum_{m_{j_1}, m_{j_2}} \sum_{m_J}$ and η is the basis label of cubic IRs and $\hat{\mathcal{O}}_{\eta}$ denotes the relative multipole basis matrices in cubic structure normalized to identity, i.e., $\text{Tr}(\hat{\mathcal{O}}_{\eta} \hat{\mathcal{O}}_{\eta}^\dagger) = 1$. The full information about O_h pairing states and their relative multipole matrices are listed in Table. II. Note that Eq. (G8) shows full correspondence between cubic point group symmetry and $SO(3)$ symmetry. To obtain the density-density interaction in the cubic field IR, we should replace $\hat{\mathcal{N}}_{J, m_J}^{S, L}(\mathbf{k})$ in Eq. (G6) with $\hat{\mathcal{N}}_{\eta}^{J, S, L}(\mathbf{k})$ in Eq. (G8). Performing a mean-field approximation with the assumption that the electron pairs have zero center of momentum, we obtain

$$\Upsilon_{\mathbf{k}}^\dagger \Upsilon_{\mathbf{k}'} \approx \langle \Upsilon_{\mathbf{k}}^\dagger | \Upsilon_{\mathbf{k}'} \rangle + \Upsilon_{\mathbf{k}}^\dagger \langle \Upsilon_{\mathbf{k}'} \rangle + \langle \Upsilon_{\mathbf{k}}^\dagger | \Upsilon_{\mathbf{k}'} \rangle, \quad (\text{G9})$$

where

$$\Upsilon_{\mathbf{k}}^\dagger \equiv c_{\mathbf{k}, m_{j_1}}^\dagger c_{-\mathbf{k}, m_{j_2}}^\dagger, \quad (\text{G10})$$

$$\Upsilon_{\mathbf{k}'} \equiv c_{-\mathbf{k}', m_{j_3}} c_{\mathbf{k}', m_{j_4}}. \quad (\text{G11})$$

In the above relations, the independency of interaction on magnetic quantum number requires $m_{j_1} = m_{j_4}$ and $m_{j_2} = m_{j_3}$. This can be clearly seen by evaluating the matrix element of interaction in two-electron state representation. The mean-field decomposition in Eq. (G9) results in an effective single particle formalism of a cubic pairing Hamiltonian in the channel (η, J, S, L)

$$H_{\eta}^{(J, S, L)} = \sum_{\mathbf{k}} \hat{c}_{\mathbf{k}}^\dagger \hat{\mathcal{H}}_{\eta}^{J, S, L}(\mathbf{k}) (\hat{c}_{-\mathbf{k}}^\dagger)^T + h.c., \quad (\text{G12})$$

with

$$\hat{\mathcal{H}}_{\eta}^{J, S, L}(\mathbf{k}) = |\mathbf{k}|^L \Delta_{\eta}^{J, S, L} \hat{\mathcal{N}}_{\eta}^{J, S, L}(\mathbf{k}) \hat{\mathcal{T}}, \quad (\text{G13})$$

where $\Delta_{\eta}^{J, S, L}$ denotes the pairing strength defined by

$$\Delta_{\eta}^{J, S, L} = \sum_{\mathbf{k}} \langle G | \hat{c}_{-\mathbf{k}}^T (|\mathbf{k}|^L \hat{\mathcal{N}}_{\eta}^{J, S, L}(\mathbf{k}) \hat{\mathcal{T}})^\dagger \hat{c}_{\mathbf{k}} | G \rangle. \quad (\text{G14})$$

with $|G\rangle$ being the superconducting ground state. Note that in the Letter, we have taken the pairing strength as a (small) constant $\Delta_{\eta}^{J, S, L} := \Delta$ for all the stationary pairing states in the weak-pairing limit.

1. Symmetry properties of inter-band pairing

In this section, we derive Eq. (9) of the main text. The Pauli exclusion principle implies that a sign change in momentum space is accompanied by exchanging the magnetic quantum numbers. This is encoded in $\hat{\mathcal{H}}_{\eta}^{J, S, L}(-\mathbf{k}) = -(\hat{\mathcal{H}}_{\eta}^{J, S, L}(\mathbf{k}))^T$, therefore, $\hat{\mathcal{N}}_{\eta}^{J, S, L}(-\mathbf{k}) \hat{\mathcal{T}} = -(\hat{\mathcal{N}}_{\eta}^{J, S, L}(\mathbf{k}) \hat{\mathcal{T}})^T$. Using these relations, we can directly find the symmetry of the inter-band pairing Hamiltonian by projecting Eq. (G13) into the inter-band subspace as

$$\begin{aligned} \hat{\Delta}_{-\mathbf{k}}^{+-} &= \hat{V}_{-\mathbf{k}}^{++} \left(|\mathbf{k}|^L \Delta_{\eta}^{J, S, L} \hat{\mathcal{N}}_{\eta}^{J, S, L}(-\mathbf{k}) \hat{\mathcal{T}} \right) \hat{V}_{\mathbf{k}}^{-\dagger T} \\ &= -\hat{V}_{-\mathbf{k}}^{++} \left(|\mathbf{k}|^L \Delta_{\eta}^{J, S, L} [\hat{\mathcal{N}}_{\eta}^{J, S, L}(\mathbf{k}) \hat{\mathcal{T}}]^T \right) \hat{V}_{\mathbf{k}}^{-\dagger T} \\ &= -[\hat{\Delta}_{\mathbf{k}}^{++}]^T, \end{aligned} \quad (\text{G15})$$

where $\hat{V}_{-\mathbf{k}}^{\pm} = \hat{V}_{\mathbf{k}}^{\pm}$ due to inversion symmetry. In the next sections, we present the explicit form of all allowed symmetry stationary s - and p -wave cubic pairings.

2. s-wave pairing in O_h symmetry

The pairing state with s -wave orbital angular momentum $L = 0$ is allowed in the even-parity A_{1g} and E_g

J	O_h	η	$\mathcal{O}_\eta(J)$	Stationary state
0	$A_{1g(u)}$	$I(f(\mathbf{r}))$	I_4	✓
1	T_{1u}	x	J_x	×
		y	J_y	×
		z	J_z	✓
2	$E_{g,u}$	$3z^2 - r^2$	$3J_z^2 - J^2$	✓
		$x^2 - y^2$	$J_x^2 - J_y^2$	✓
	$T_{2g,u}$	xy	$[J_x J_y]$	×
		zx	$[J_z J_x]$	×
3	A_{2u}	xyz	$[J_x J_y J_z]$	✓
		x^3	J_x^3	×
	T_{1u}	y^3	J_y^3	×
		z^3	J_z^3	×
	T_{2u}	$z(x^2 - y^2)$	$[J_z(J_x^2 - J_y^2)]$	×
		$x(y^2 - z^2)$	$[J_x(J_y^2 - J_z^2)]$	×
		$y(z^2 - x^2)$	$[J_y(J_z^2 - J_x^2)]$	×

Table II. Time-reversal pairing states in cubic point group symmetry. The first and second columns identify the correspondence between total angular momentum of pairing states and IRs of the O_h symmetry [51, 52]. The real space basis of each IR is denoted in the third column with their corresponding J basis in the fourth column. Here, the square brackets [...] symmetrize the multipole basis operator $[\hat{A}\hat{B}] = (\hat{A}\hat{B} + \hat{B}\hat{A})/2!$ and $[\hat{A}\hat{B}\hat{C}] = (\hat{A}\hat{B}\hat{C} + \hat{A}\hat{C}\hat{B} + \hat{B}\hat{C}\hat{A} + \hat{B}\hat{A}\hat{C} + \hat{C}\hat{A}\hat{B} + \hat{C}\hat{B}\hat{A})/3!$. In the last column, ✓ (×) implies that the pairing state is (is not) the stationary state of the free energy [9].

channels. Here, we derive the cubic pairing states corresponding to the relative allowed symmetry quantum numbers (J, S, L) . The even-parity A_{1g} state in the channel $(0, 0, 0)$ and E_g states in the channel $(2, 2, 0)$ are given by

$$\hat{N}_I^{0,0,0}(\mathbf{k}) = \hat{N}_{0,0}^{0,0}(\mathbf{k}), \quad (\text{G16})$$

$$\hat{N}_{3z^2-r^2}^{2,2,0}(\mathbf{k}) = \hat{N}_{2,0}^{2,0}(\mathbf{k}), \quad (\text{G17})$$

$$\hat{N}_{x^2-y^2}^{2,2,0}(\mathbf{k}) = \frac{1}{\sqrt{2}} \left(\hat{N}_{2,-2}^{2,0}(\mathbf{k}) + \hat{N}_{2,2}^{2,0}(\mathbf{k}) \right). \quad (\text{G18})$$

Inserting the above relations into Eq. (G13), this results in the explicit matrix formalism of the pairing Hamiltonians as

$$\hat{\mathcal{H}}_I^{0,0,0}(\mathbf{k}) = \Delta_I^{0,0,0} \begin{pmatrix} 0 & 0 & 0 & 1 \\ 0 & 0 & -1 & 0 \\ 0 & 1 & 0 & 0 \\ -1 & 0 & 0 & 0 \end{pmatrix}, \quad (\text{G19})$$

$$\hat{\mathcal{H}}_{3z^2-r^2}^{2,2,0}(\mathbf{k}) = \Delta_{3z^2-r^2}^{2,2,0} \begin{pmatrix} 0 & 0 & 0 & 1 \\ 0 & 0 & 1 & 0 \\ 0 & -1 & 0 & 0 \\ -1 & 0 & 0 & 0 \end{pmatrix}, \quad (\text{G20})$$

$$\hat{\mathcal{H}}_{x^2-y^2}^{2,2,0}(\mathbf{k}) = \Delta_{x^2-y^2}^{2,2,0} \begin{pmatrix} 0 & 1 & 0 & 0 \\ -1 & 0 & 0 & 0 \\ 0 & 0 & 0 & 1 \\ 0 & 0 & -1 & 0 \end{pmatrix}. \quad (\text{G21})$$

3. p -wave pairing in O_h symmetry

The p -wave gap functions implies that $L = 1$. Therefore, the superconducting gap functions depend linearly on momentum. Since the orbital angular momentum is odd, consequently, the intrinsic spin part of Cooper pairs should be odd due to Fermi statistics. Therefore, the p -wave gap functions are odd in momentum implying that $\hat{\mathcal{H}}_\eta^{J,S,L}(-\mathbf{k}) = -\hat{\mathcal{H}}_\eta^{J,S,L}(\mathbf{k})$. Taking into account the condition $|S - L| \leq J \leq |S + L|$, the odd parity p -wave Cooper pairing can possess either spin dipole structure $S = 1$ or spin octupole structure $S = 3$. Hence, Cooper pairs can have singlet $J = 0$, triplet $J = 1$, and quintet $J = 2$ total angular momenta for spin dipole moment. Also, quintet $J = 2$ and septet $J = 3$ total angular momenta correspond to pairing with spin octupole structure. It is worth mentioning that the triplet and septet pairings can only happen in the p -wave channel. In the following, we obtain the explicit matrix formalism of Hamiltonians describing p -wave pairings in O_h point group symmetry. This can be done by inserting Eq. (G8) into Eq. (G13).

a. Singlet state $J = 0$

Here, we derive the odd-parity pairing state A_{1u} . The symmetry constraint allows for the channel $(0, 1, 1)$. The J representation of the A_{1u} state and the full matrix formalism of pairing results in

$$\hat{N}_{f(\mathbf{r})}^{0,1,1}(\mathbf{k}) = \hat{N}_{0,0}^{1,1}(\mathbf{k}),$$

$$\hat{\mathcal{H}}_{f(\mathbf{r})}^{0,1,1}(\mathbf{k}) = \Delta_{f(\mathbf{r})}^{0,1,1} \begin{pmatrix} 0 & 0 & -\frac{\sqrt{3}}{2}k_- & \frac{3k_z}{2} \\ 0 & k_- & -\frac{1}{2}k_z & \frac{\sqrt{3}}{2}k_+ \\ -\frac{\sqrt{3}}{2}k_- & -\frac{1}{2}k_z & -k_+ & 0 \\ \frac{3k_z}{2} & \frac{\sqrt{3}}{2}k_+ & 0 & 0 \end{pmatrix}. \quad (\text{G22})$$

b. Triplet state $J = 1$

In the cubic field, the $J = 1$ state is labeled by the T_{1u} IR which is a three-fold degenerate state, each denoted by the basis $\eta = x, y, z$. Note that only $\eta = z$ is a stationary state of the free energy preserving time-reversal symmetry [9, 64]. Hence, we focus on it. The total angular momentum representation of this state which lies in the channel $(1, 1, 1)$ is

$$\hat{N}_z^{1,1,1}(\mathbf{k}) = \hat{N}_{1,0}^{1,1}(\mathbf{k}). \quad (\text{G23})$$

The full matrix of the odd-parity triplet pairing takes the form

$$\hat{\mathcal{H}}_z^{1,1,1}(\mathbf{k}) = \Delta_z^{1,1,1} \begin{pmatrix} 0 & 0 & k_- & 0 \\ 0 & -\frac{2}{\sqrt{3}}k_- & 0 & k_+ \\ k_- & 0 & -\frac{2}{\sqrt{3}}k_+ & 0 \\ 0 & k_+ & 0 & 0 \end{pmatrix}. \quad (\text{G24})$$

c. Quintet state $J = 2$

Here, we derive the odd-parity pairing states with E_u and T_{2u} IR corresponding to states with quintet total angular momentum. It is worth mentioning that the J representation of these IR are the same as Eqs. (G20)-(G21). We represent them for ($S = 1, L = 1$) and ($S = 3, L = 1$) channels. The pairing Hamiltonian of the former channel takes the form

$$\hat{\mathcal{H}}_{3z^2-r^2}^{2,1,1}(\mathbf{k}) = \Delta_{3z^2-r^2}^{2,1,1} \begin{pmatrix} 0 & 0 & \frac{\sqrt{3}}{2}k_- & 3k_z \\ 0 & -k_- & -k_z & -\frac{\sqrt{3}}{2}k_+ \\ \frac{\sqrt{3}}{2}k_- & -k_z & k_+ & 0 \\ 3k_z & -\frac{\sqrt{3}}{2}k_+ & 0 & 0 \end{pmatrix}. \quad (\text{G25})$$

$$\hat{\mathcal{H}}_{x^2-y^2}^{2,1,1}(\mathbf{k}) = \Delta_{x^2-y^2}^{2,1,1} \begin{pmatrix} 0 & 0 & -k_+ & 0 \\ 0 & \frac{2}{\sqrt{3}}k_+ & 0 & k_- \\ -k_+ & 0 & -\frac{2}{\sqrt{3}}k_- & 0 \\ 0 & k_- & 0 & 0 \end{pmatrix}. \quad (\text{G26})$$

Moreover, the quintet Hamiltonians with spin octupole $S = 3$ structures are given by

$$\hat{\mathcal{H}}_{3z^2-r^2}^{2,3,1}(\mathbf{k}) = \Delta_{3z^2-r^2}^{2,3,1} \begin{pmatrix} 0 & 0 & \frac{1}{\sqrt{3}}k_- & -\frac{1}{2}k_z \\ 0 & k_- & -\frac{3}{2}k_z & \frac{1}{\sqrt{3}}k_+ \\ \frac{1}{\sqrt{3}}k_- & -\frac{3}{2}k_z & -k_+ & 0 \\ -\frac{1}{2}k_z & \frac{1}{\sqrt{3}}k_+ & 0 & 0 \end{pmatrix}. \quad (\text{G27})$$

$$\hat{\mathcal{H}}_{x^2-y^2}^{2,3,1}(\mathbf{k}) = \Delta_{x^2-y^2}^{2,3,1} \begin{pmatrix} 5\sqrt{3}k_- & -5k_z & -k_+ & 0 \\ -5k_z & -\sqrt{3}k_+ & 0 & k_- \\ -k_+ & 0 & \sqrt{3}k_- & -5k_z \\ 0 & k_- & -5k_z & -5\sqrt{3}k_+ \end{pmatrix}. \quad (\text{G28})$$

d. Septet state $J = 3$

The p -wave septet $J = 3$ state in cubic representation decomposes into $A_{2u} + T_{1u} + T_{2u}$ IR [51, 52]. In this case, the Cooper pairs have only intrinsic spin octupole structure $S = 3$. The A_{2u} state [6] is a stationary state [9] and its matrix Hamiltonian is given by

$$\hat{N}_{xyz}^{3,3,1}(\mathbf{k}) = \frac{1}{i\sqrt{2}} \left(\hat{\mathcal{N}}_{3,2}^{3,1}(\mathbf{k}) - \hat{\mathcal{N}}_{3,-2}^{3,1}(\mathbf{k}) \right), \quad (\text{G29})$$

$$\hat{\mathcal{H}}_{xyz}^{3,3,1}(\mathbf{k}) = \Delta_{xyz}^{3,3,1} \begin{pmatrix} \frac{3}{4}k_- & \frac{\sqrt{3}}{2}k_z & \frac{\sqrt{3}}{4}k_+ & 0 \\ \frac{\sqrt{3}}{2}k_z & \frac{3}{4}k_+ & 0 & -\frac{\sqrt{3}}{4}k_- \\ \frac{\sqrt{3}}{4}k_+ & 0 & -\frac{3}{4}k_- & \frac{\sqrt{3}}{2}k_z \\ 0 & -\frac{\sqrt{3}}{4}k_- & \frac{\sqrt{3}}{2}k_z & -\frac{3}{4}k_+ \end{pmatrix}. \quad (\text{G30})$$

Appendix H: Multipole matrices in $j = 3/2$ representation

The multipole matrix for $S = 1$ and $S = 3$ with the highest m_S quantum numbers are

$$\hat{S}_{1,1} = \begin{pmatrix} 0 & \frac{-\sqrt{3}}{\sqrt{10}} & 0 & 0 \\ 0 & 0 & \frac{-\sqrt{2}}{\sqrt{5}} & 0 \\ 0 & 0 & 0 & \frac{\sqrt{3}}{\sqrt{10}} \\ 0 & 0 & 0 & 0 \end{pmatrix}, \quad \hat{S}_{3,3} = \begin{pmatrix} 0 & 0 & 0 & -1 \\ 0 & 0 & 0 & 0 \\ 0 & 0 & 0 & 0 \\ 0 & 0 & 0 & 0 \end{pmatrix}. \quad (\text{H1})$$

Furthermore, the spherical harmonic for $L = 1$ are $|\mathbf{k}|Y_{1,\pm 1} = \mp\sqrt{3/8\pi}k_{\pm}$ and $|\mathbf{k}|Y_{1,0} = \sqrt{3/4\pi}k_z$. The \hat{J}_i (\hat{S}_i) matrices with $i \in \{x, y, z\}$ in $j = 3/2$ basis are given by

$$\hat{J}_x = \hat{S}_x = \frac{\hbar}{2} \begin{pmatrix} 0 & \sqrt{3} & 0 & 0 \\ \sqrt{3} & 0 & 2 & 0 \\ 0 & 2 & 0 & \sqrt{3} \\ 0 & 0 & \sqrt{3} & 0 \end{pmatrix}, \quad (\text{H2})$$

$$\hat{J}_y = \hat{S}_y = \frac{\hbar}{2} \begin{pmatrix} 0 & -i\sqrt{3} & 0 & 0 \\ i\sqrt{3} & 0 & -i2 & 0 \\ 0 & i2 & 0 & -i\sqrt{3} \\ 0 & 0 & i\sqrt{3} & 0 \end{pmatrix}, \quad (\text{H3})$$

$$\hat{J}_z = \hat{S}_z = \frac{\hbar}{2} \begin{pmatrix} 3 & 0 & 0 & 0 \\ 0 & 1 & 0 & 0 \\ 0 & 0 & -1 & 0 \\ 0 & 0 & 0 & -3 \end{pmatrix}. \quad (\text{H4})$$